Paleoceanography and Paleoclimatology

RESEARCH ARTICLE
10.1029/2018PA003417

Considerations for *Globigerinoides ruber* (White and Pink) Paleoceanography: Comprehensive Insights From a Long-Running Sediment Trap

Julie N. Richey[1], Kaustubh Thirumalai[2,3], Deborah Khider[3,4], Caitlin E. Reynolds[1], Judson W. Partin[3], and Terrence M. Quinn[3]

[1]U.S. Geological Survey, St. Petersburg, FL, USA, [2]Department of Earth, Environmental, and Planetary Sciences, Brown University, Providence, RI, USA, [3]Institute for Geophysics, Jackson School of Geosciences, University of Texas at Austin, Austin, TX, USA, [4]Information Sciences Institute, University of Southern California, Los Angeles, CA, USA

Key Points:
- There is no difference in the depth habitat or seasonal distribution of pink and white chromotypes of *G. ruber* in the modern GoM
- *G. ruber* chromotypes display the same morphological variants, suggesting evidence for the preclusion of divergent evolution between pink *G. ruber* and *sl* morphotype
- New $\delta^{18}O_{sw}$-salinity relationships for the northern GoM are generated from paired water column measurements over the course a decade

Supporting Information:
- Supporting Information S1

Correspondence to:
J. N. Richey,
jrichey@usgs.gov

Citation:
Richey, J. N., Thirumalai, K., Khider, D., Reynolds, C. E., Partin, J. W., & Quinn, T. M. (2019). Considerations for *Globigerinoides ruber* (white and pink) paleoceanography: Comprehensive insights from a long-running sediment trap. *Paleoceanography and Paleoclimatology*, *34*, 353–373. https://doi.org/10.1029/2018PA003417

Received 11 JUN 2018
Accepted 25 JAN 2019
Accepted article online 6 FEB 2019
Published online 18 MAR 2019

Abstract We present a detailed analysis of the seasonal distribution, size, morphological variability, and geochemistry of co-occurring pink and white chromotypes of *Globigerinoides ruber* from a high-resolution (1–2 weeks) and long-running sediment trap time series in the northern Gulf of Mexico. We find no difference in the seasonal flux of the two chromotypes. Although flux of *G. ruber* is consistently lowest in winter, the flux-weighted signal exported to marine sediments represents mean annual conditions in the surface mixed layer. We observe the same morphological diversity among pink specimens of *G. ruber* as white. Comparison of the oxygen and carbon isotopic composition ($\delta^{18}O$ and $\delta^{13}C$) of two morphotypes (*sensu stricto* and *sensu lato*) of pink *G. ruber* reveals the isotopes to be indistinguishable. The test size distribution within the population varies seasonally, with the abundance of large individuals increasing (decreasing) with increasing (decreasing) sea surface temperature. We find no systematic offsets in the Mg/Ca and $\delta^{18}O$ of co-occurring pink and white *G. ruber*. The sediment trap data set shows that the Mg/Ca-temperature sensitivity for both chromotypes is much lower than the canonical 9%/°C, which can likely be attributed to the secondary influence of both salinity and pH on foraminiferal Mg/Ca. Using paired Mg/Ca and $\delta^{18}O$, we evaluate the performance of a suite of published equations for calculating sea surface temperature, sea surface salinity, and isotopic composition of seawater ($\delta^{18}O_{sw}$), including a new salinity-$\delta^{18}O_{sw}$ relationship for the northern Gulf of Mexico from water column observations.

1. Introduction

The development of quantitatively well-constrained reconstructions of hydrographic parameters like sea surface temperature (SST) and sea surface salinity (SSS) using marine sediment cores is essential to advancing knowledge on multidecadal and centennial climate variability (e.g., changes in the Atlantic Meridional Overturning Circulation and the Atlantic Multidecadal Oscillation) and to quantifying mean shifts in oceanographic parameters on longer timescales (e.g., orbital to tectonic timescales). Calibration and verification of geochemical proxies via sediment trap studies provides the opportunity to evaluate assumptions about the ecology of proxy recorders such as planktic foraminifera and also to validate transfer functions used to calculate physical parameters (e.g., temperature, salinity, and pH) from foraminiferal geochemistry. In this study, we focus on the paired magnesium-to-calcium ratio (Mg/Ca) and oxygen isotopic composition of calcite ($\delta^{18}O_c$) of both pink and white *Globigerinoides ruber* in the northern Gulf of Mexico (nGoM), a region particularly well suited for high-resolution paleoceanographic reconstruction in the Quaternary period (Antonarakou et al., 2015; Flower et al., 2004; LoDico et al., 2006; Nürnberg et al., 2008; Richey et al., 2007, 2009; Thirumalai et al., 2018; Williams et al., 2010). The continental slope of the nGoM is punctuated with deep basins (>1,000 m) that have rapid sediment accumulation rates due to the large influx of terrigenous material delivered via the Mississippi River. The combination of high sedimentation rates, concurrent deposition of both marine and terrestrial material, and proximity to Mississippi River discharge makes the nGoM an ideal location for assessing linkages between continental and marine climate change (Hill et al., 2006; Meckler et al., 2008; Richey et al., 2011; Thirumalai et al., 2018)

The planktic foraminifer, *G. ruber*, has a cosmopolitan distribution in the tropical to midlatitude oceans, and its geochemistry is widely used as a proxy recorder of changes in mean annual SST and SSS. It is well suited for paleoceanographic reconstruction of surface hydrographic conditions because both its oxygen isotopic

composition (Anand et al., 2003; Venancio et al., 2017) and its distribution in depth-stratified plankton tows (e.g., Jentzen et al., 2018; Schmuker & Schiebel, 2002) indicate that it completes its life cycle within the near-surface part of the water column (0–50 m). *Globigerinoides ruber* is abundant, making up 20%–40% of the planktic foraminiferal assemblage in the low to midlatitude Atlantic Ocean (Tolderlund & Bé, 1971), and is the dominant species found in the oligotrophic surface waters of the subtropical gyres (Bé & Tolderlund, 1971; Lombard et al., 2011; Storz et al., 2009). *Globigerinoides ruber* is composed of a gradient of morphological variants which co-occur in sediments and the water column (Aurahs et al., 2009). Among these variants are the white and pink chromotypes, the latter of which contains pink pigmentation in the test. This pigmentation ranges from a pale pink spot only visible on the early ontogenetic chambers to bright pink pigmentation over the entire final whorl. The pink chromotype disappeared from the Indian Ocean ca. 120 kyr BP (Thompson et al., 1979), although it has recently been reported in modern Indian Ocean sediments (Bhattacharjee et al., 2013).

Within the white chromotype, a range of morphometric variability has been reported, with two primary morphotypes having been identified in paleoceanographic applications. The morphotype with a compressed, subspherical final chamber is often referred to as *sensu lato* (*sl*, also *Globigerinoides elongatus*, or *Globigerinoides ruber pyramidalis*), while the morphotype with a larger, more spherical and symmetrical final chamber is identified as *sensu stricto* (*ss*, also normalform or *Globigerinoides ruber ruber*; Aurahs et al., 2011; Sadekov et al., 2008; Wang, 2000). Molecular genetic analysis suggests that the *sl* morphotype is genetically distinct from the *ss* morphotype and that the pink chromotype of *G. ruber* has a genotype more closely related to the *ss* morphotype of *G. ruber* (Aurahs et al., 2011). Although, it is important to note that in Aurahs et al. (2011), the pink *G. ruber* specimens analyzed for genetics were morphologically similar to the white *ss* variety. In the white morphotype, some studies have found offsets in the Mg/Ca, $\delta^{18}O$, and $\delta^{13}C$ of co-occurring *ss* and *sl* specimens (Antonarakou et al., 2015; Steinke et al., 2005; Wang, 2000). However, Thirumalai et al. (2014) demonstrated, using the same nGoM sediment trap sample set from this study and core tops and down core samples, that there is no systematic difference between the isotopic composition of *ss* and *sl* morphotypes of co-occurring white *G. ruber*. Similarly, Gray et al. (2018) found no difference in the Mg/Ca of *ss* and *sl G. ruber* in the tropical Atlantic and Indian Oceans.

Although there is a wealth of available literature on the life history, geochemistry, and distribution of *G. ruber* in the global ocean, a detailed comparison of the pink and white chromotypes has not been performed to test assumptions about differences in their seasonality, depth distribution, and geochemistry. In this study we address the seasonal flux, morphological variability, and shell geochemistry of the two chromotypes of *G. ruber* from a long-running sediment trap time series in the nGoM. This location is well suited for addressing these questions, as this site experiences a large seasonal SST cycle (~10 °C), and relatively large foraminiferal flux, allowing for high temporal resolution. Details regarding the seasonal variations in flux and geochemistry of paleoceanographically relevant proxies from this nGoM sediment trap time series have been published in Richey and Tierney (2016) (alkenones and isoprenoid glycerol dibiphytanyl glycerol tetraethers) and Reynolds et al. (2018; planktic foraminifer, *Globorotalia truncatulinoides*). Using seasonally resolved paired measurements of Mg/Ca and $\delta^{18}O_c$, we are also able to assess the relationship between temperature, salinity, and shell geochemistry in both pink and white *G. ruber*, as well as potential differences between the two chromotypes. We quantitatively compare the accuracy of different combinations of transfer functions for deriving SST, $\delta^{18}O_{sw}$, and SSS from paired Mg/Ca and $\delta^{18}O_c$ measurements in *G. ruber*. Ultimately, we are able to recommend a set of best practices for applying paired Mg/Ca and $\delta^{18}O_c$ analyses of *G. ruber* for paleoceanographic reconstructions. These include appropriate a priori assumptions about *G. ruber* ecology, and the combination of equations that most accurately reflects mean annual SST, SSS, and $\delta^{18}O_{sw}$ based on modern observations.

2. Regional Setting

The Gulf of Mexico (GoM) is a semienclosed basin in the subtropical North Atlantic Ocean. A feature known as the Loop Current, in which warm salty Caribbean water enters the GoM through the Yucatan Straits and exits through the Florida Straits to join the Gulf Stream, connects the GoM with the tropical and subtropical Atlantic Ocean. The northern and western extent of the Loop Current fluctuates seasonally, with the maximum penetration into the GoM occurring in summer (Lindo-Atichati et al., 2013). Warm-core or

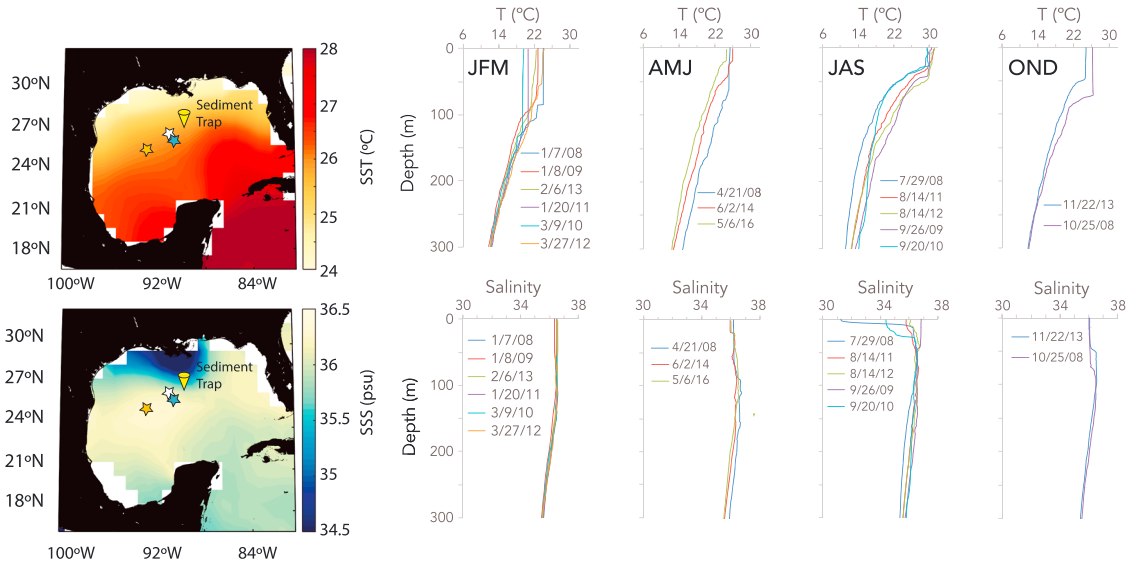

Figure 1. Location of the sediment trap (yellow cone) and the Gulf of Mexico coring locations referenced in the discussion (Pigmy Basin-white star, Orca Basin-blue star, and Garrison Basin-orange star) are shown on a map of mean annual SST (HadISST; Rayner et al., 2003) and mean annual SSS (ORA-S4; Balmaseda et al., 2013). Shown on the right are vertical temperature and salinity profiles of the upper 300 m of the water column from CTD casts at the sediment trap site 2008–2013. Profiles are grouped seasonally into winter (JFM, January–March), spring (AMJ, April–June), summer (JAS, July–September), and fall (OND, October–December).

anticyclonic eddies sporadically separate from the Loop Current and propagate warm salty water into the northern and western GoM. This process is quasiperiodic, with an eddy shedding period of 11 (±4) months (Vukovich, 2007). These warm-core eddies are characterized by an anomalously deep and warm mixed layer. Cold-core or cyclonic eddies are characterized by anomalously cold and fresh surface water, due to entrainment of water from the shelf and upwelling (Huang et al., 2013; Lee et al., 1995; Walker et al., 2011).

The sediment trap is situated in the nGoM (27.5°N, 90.3°W), 200 km southwest of the Mississippi River delta, on the continental slope (Figure 1). Monthly mean SSTs vary between 19 °C and 31 °C. There is good agreement between monthly SSTs observed from a local buoy in Green Canyon (205a; http://www.ndbc.noaa.gov), gridded SST from the HadISST data set (Rayner et al., 2003), and CTD observations (Figure 1). Sea surface salinity generally varies between 35 and 37 psu, with the maximum in winter and minimum in summer. Mississippi River plume waters do not reach the outer continental slope where our sediment trap mooring is located, but mesoscale eddies can entrain low-salinity waters from the continental shelf and cause short-term low-salinity anomalies in the surface mixed layer (Huang et al., 2013; Walker et al., 2011). For example, during a cruise to the sediment trap site in September 2010, an anomalously low salinity (34.4 psu) was observed in the upper 10–20 m of the water column, and satellite altimetry data indicate the presence of a *cold-core* or cyclonic eddy over the sediment trap site in September 2010. This salinity anomaly is 1.5 (±0.1) psu lower than the salinity observed in August of 2011 and 2012. The ORA-S4 gridded salinity product shows a salinity range of 34.3 to 36.3 psu between 2008 and 2014, with minima that drop below 35 psu each summer (Balmaseda et al., 2013). The gridded SSS data are overall lower than our CTD surface salinity observations at the sediment trap site, which vary between 34.8 and 36.8 psu (Figure S1, supporting information). Although our CTD measurements at the sediment trap site likely undersample the annual range, we have midsummer salinity observations in 2009, 2011, and 2012 that indicate SSS > 36 psu, suggesting that salinity minima <36 psu are sporadic, and not necessarily an annual feature at this site.

3. Methods

3.1. Sediment Trap

The sediment trap mooring (McLane PARFLUX Mark 78) was deployed in January 2008 in the nGoM (27.5°N, 90.3°W) in 1,150-m water depth. The trap was positioned in the water column at a depth of 700 m on the mooring cable to enable the collection of deeper dwelling species of planktic foraminifera.

The trap contains 21 collection cups that are programmed to rotate every 7 to 14 days (resulting in weekly to biweekly sampling resolution). Sample cups are filled with a high-density buffered solution (salinity = ~44 psu) made with formalin (3.7%), sodium borate, and filtered seawater. A gap in sampling occurred from the beginning of February to late March 2012. Bulk sediment flux parameters (e.g., mass flux, organic carbon flux, biogenic silica flux, and particulate nitrogen flux) for the interval 2008–2012 can be found in Richey et al. (2014).

3.2. Foraminiferal Picking

Samples were wet split into four aliquots using a precision rotary splitter, stored in buffered deionized water, and refrigerated. A quarter split was wet sieved over a 150 μm sieve and subsequently wet picked for all foraminifers. In samples containing fewer than 300 foraminifers in the first quarter split, an additional split was processed and picked. The counts were then summed. All planktic foraminifers were identified to the species level. The species counts are reported as flux in tests per square meter per day (m^2/day). Flux was calculated by multiplying the individual species counts by number of splits, then dividing by the total duration of the sampling period, which was typically 7 or 14 days. Total foraminiferal assemblage fluxes for the interval 2008–2011 are reported in Poore et al. (2013), and the flux data set is extended through 2014 in Reynolds and Richey (2016).

All individuals used for geochemical analysis were picked from the 212–425-μm size range. For the 2010 samples, two different size fractions were analyzed (212–300 and 300–425 μm), when a sufficient number of foraminifera were present. For the 2011–2013 samples, each individual foraminifer was measured along two axes (length and width) and identified as *ss*, *sl*, or intermediate (a designation for individuals that do not fit the criteria for holotypic *ss* or *sl*). Details on the morphology associated with each type can be found in Thirumalai et al. (2014). We looked at the relationship between Mg/Ca and test size in a sample from September 2011, when *G. ruber* flux was exceptionally high. Three aliquots of 100 white *G. ruber* were picked, cleaned, and analyzed separately from four size fractions (150–212, 212–250, 250–300, and 300–355 μm). We repeated the experiment with pink *G. ruber* using four size fractions (212–250, 250–300, 300–355, and 355–425 μm).

3.3. Elemental and Isotopic Analysis of Foraminifera

Overall, 67 (74) isotopic and 60 (81) Mg/Ca determinations were made on white (pink) *G. ruber* from 2010 to 2013, with 54 (70) of those being paired measurements (Mg/Ca and $\delta^{18}O$ on the same sample). For elemental analyses, 30–60 foraminifera from the 212–425-μm size fraction were lightly crushed, homogenized, and cleaned according to a modified version of the Barker et al. (2003) protocol. Briefly, the cleaning procedure included two Milli-Q water rinses, two methanol rinses, an oxidation step with a modified buffered hydrogen peroxide solution following Russell et al. (2004) for recently living foraminifer (1:1 solution of 0.1 N NaOH and 30% H_2O_2), and a dilute acid leach (0.001 M nitric acid). A reductive cleaning step was not performed, as these foraminifers were not subject to diagenetic Fe-Mn oxide coatings often found on foraminifera from sediment cores (Boyle, 1981; Boyle & Keigwin, 1985; Lea & Boyle, 1991). Cleaned foraminiferal samples collected in 2011–2013 were dissolved in nitric acid to achieve a target calcium concentration of 20 ppm. Acidified samples were analyzed on a PerkinElmer 7300 DV inductively coupled optical emission spectrometer (ICP-OES) at the USGS St. Petersburg Coastal and Marine Science Center, FL, USA. Mg/Ca was corrected for instrumental drift using the internal gravimetric standard (IGS) method devised by Schrag (1999). The average-corrected IGS precision for Mg/Ca was 0.024 mmol/mol (1σ, $n = 1{,}315$). A $CaCO_3$ standard (homogenized powder of ECRM-751) analyzed for Mg/Ca to test for any potential matrix effects had an average corrected precision of 0.096 mmol/mol (1σ, $n = 123$). We analyzed the JCt-1 standard used in an interlaboratory comparison study of Mg/Ca and determined an average Mg/Ca of 1.228 ± 0.037 mmol/mol ($n = 10$, 1σ), within 2σ error of the mean value of 1.289 mmol/mol reported in Hathorne et al. (2013). Samples from 2010 were cleaned according to the Barker et al. (2003) procedure in a laminar flow clean bench and analyzed for Mg/Ca and Ba/Ca using inductively coupled plasma mass spectrometry at Texas A&M, College Station, Texas, USA on a Thermo Scientific Element XR High Resolution ICP-MS.

Carbon and oxygen isotopic analyses were performed on aliquots of six to eight whole foraminifera shells (212–425 μm), on a Thermo-Finnigan MAT 253 isotope ratio mass spectrometer coupled to a Kiel IV Carbonate Device housed in the Analytical Laboratory for Paleoclimate Studies at the Jackson School of

Geosciences, University of Texas at Austin, Austin, Texas, USA. The 1σ precision of stable isotopic measurements in this study is based on multiple analyses of an in-house carbonate standard (n = 24) is 0.03‰ for $\delta^{13}C$ and 0.06‰ for $\delta^{18}O$, consistent with long-term precision for this instrumental setup (0.06‰ for $\delta^{13}C$ and 0.08‰ for $\delta^{18}O$). All stable isotope values are reported relative to Vienna Pee Dee Belemnite.

3.4. Isotopic Analysis of Seawater

A total of 189 seawater samples were collected from Niskin bottles during CTD casts on 17 sediment trap deployment/recovery cruises from 2008 to 2017. The oxygen isotopic composition of seawater was measured on a Gasbench coupled to a MAT 253 isotope ratio mass spectrometer at the University of Texas at Austin, Austin, Texas, USA, where the long-term precision of replicate measurements of an in-house standard was 0.12‰ and 2‰ for $\delta^{18}O$ and $\delta^{2}H$, respectively (2σ). Samples collected after 2010 were analyzed for both hydrogen ($\delta^{2}H$) and oxygen ($\delta^{18}O$) composition on a Picarro L2130-i Isotopic Liquid Water Analyzer (Picarro, Inc. Santa Clara, CA) at the University of Texas at Austin, Austin, Texas, USA. All isotopic values are given relative to Vienna Standard Mean Ocean Water (VSMOW). The long-term precision of replicate measurements of an in-house standard on the Picarro L2130-i was 0.13‰ and 0.59‰ for $\delta^{18}O$ and $\delta^{2}H$, respectively.

4. Results and Discussion

4.1. Salinity-$\delta^{18}O_{seawater}$ Relationship in the Northern Gulf of Mexico

The ability to quantitatively reconstruct salinity from paired Mg/Ca-$\delta^{18}O_c$ measurements on planktic foraminifera is dependent on a robust regional $\delta^{18}O_{sw}$-salinity relationship. This relationship has been demonstrated to vary both regionally (Conroy et al., 2017; LeGrande & Schmidt, 2006) and temporally within a region (Conroy et al., 2017; Wagner & Slowey, 2011). LeGrande and Schmidt (2006) published $\delta^{18}O_{sw}$-salinity relationships for the tropical Atlantic Ocean and North Atlantic Ocean from a global gridded database of $\delta^{18}O_{sw}$ based on observations; however, no direct observations of $\delta^{18}O_{sw}$ from the GoM were available for the database. Wagner and Slowey (2011) published $\delta^{18}O_{sw}$-salinity relationships for the continental shelf in the nGoM, with an offshore end-member at the Flower Garden Banks. The slope of their summer $\delta^{18}O_{sw}$-salinity relationship is identical to the slope of the tropical Atlantic equation (0.15 $\pm$ 0.01) of LeGrande and Schmidt (2006).

Paired salinity-$\delta^{18}O_{sw}$ measurements are available from CTD casts on 15 cruises to the offshore nGoM sediment trap site from 2008 to 2016. A total of 167 samples from the surface to 1,200-m water depth are included in this data set. Figure 2 shows the entire data set with the aforementioned salinity-$\delta^{18}O_{sw}$ relationships for reference. We use a weighted linear regression with bivariate error (Thirumalai et al., 2011) to regress $\delta^{18}O_{sw}$ against salinity for the entire data set (0–1,200 m) and a separate simple linear regression for samples that were collected within the surface mixed layer (the mixed-layer depth was determined for each sampling trip, based on CTD temperature profiles). The mixed-layer equation (n = 33) has a slope (0.20 $\pm$ 0.03) that is within 1σ uncertainty of the spring GoM continental shelf equation published by Wagner and Slowey (2011) and within 2σ of the slope for the tropical Atlantic published by LeGrande and Schmidt (2006).

While the majority of surface mixed-layer samples had a salinity >36 psu, there were three observations of surface salinities below 36 psu. All come from a single cruise on 20 September 2010, when there was a low-salinity anomaly in the upper 30 m of the water column. This is likely due to the presence of a cyclonic or cold-core eddy at the sediment trap site on 20 September 2010 (http://www.aoml.noaa.gov/phod/dhos/altimetry.php), which potentially entrained low-salinity Mississippi River water from the shelf (Walker et al., 2011). The slope of the mixed-layer $\delta^{18}O_{sw}$-salinity relationship is largely driven by these three low-salinity observations. A linear mixing model with a Caribbean-surface-water end-member (salinity = 36.1; $\delta^{18}O_{sw}$ = 1.12‰; from https://data.giss.nasa.gov/o18data/, Schmidt et al., 1999) and Mississippi-River-water end-member (salinity = 0; $\delta^{18}O_{sw}$ = −6.63‰; from Coplen & Kendall, 2000) yields a slope of 0.21, which is indistinguishable from the slope of the surface mixed-layer $\delta^{18}O_{sw}$-salinity relationship presented in this study. We assume that the slope of this surface mixed-layer equation is driven by the Mississippi River end-member, and therefore, it is most appropriate to use this relationship at nGoM sites that are susceptible to entrainment of Mississippi River discharge; the $\delta^{18}O_{sw}$-salinity relationship likely has a larger slope in the

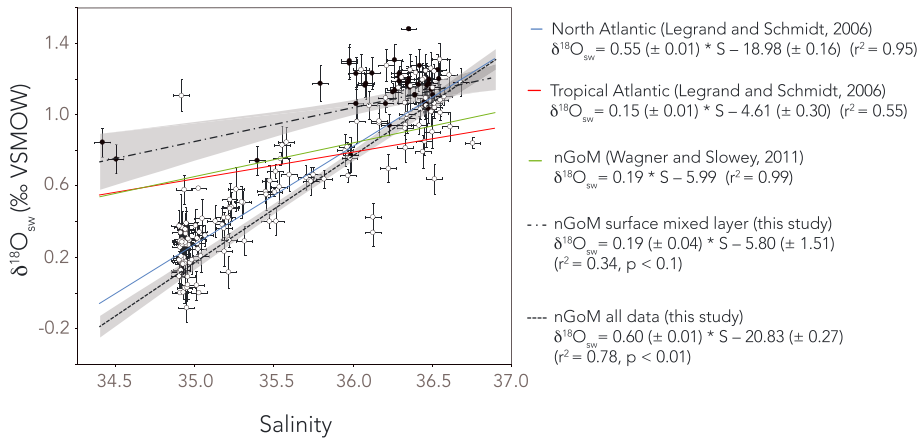

Figure 2. Salinity-$\delta^{18}O_{sw}$ relationship for the nGoM. Paired measurements of the oxygen isotopic composition of seawater and salinity from 15 CTD casts spanning 2008–2017 and from the surface to 1,200-m water depth. The regression based on all data includes data indicated with both open and closed circles ($n = 189$). Data from surface mixed-layer samples (0–25 m in summer and 0–130 m in winter) are shown with closed circles ($n = 41$). Vertical error bars are analytical uncertainty in $\delta^{18}O_{sw}$ measurements, and horizontal error bars represent a conservative uncertainty estimate of 0.05 psu on the CTD salinity sensor, an order of magnitude higher than estimated by Ingleby and Huddleston (2007). Regressions based on this nGoM mixed-layer data (black dashed line) and the 0–1,200-m data (gray dashed line) are shown with 95% confidence intervals shaded in gray. Published salinity-$\delta^{18}O_{sw}$ relationships are shown in blue (North Atlantic equation; LeGrande & Schmidt, 2006), red (tropical Atlantic equation; LeGrande & Schmidt, 2006), and green (Flower Garden Banks, Gulf of Mexico equations; Wagner & Slowey, 2011).

central and western GoM, and thus, it may be more appropriate to use an equation with a slope closer to 0.6‰ per psu.

4.2. Flux

On average, *G. ruber* comprises 31% of the total planktic foraminiferal assemblage in the nGoM sediment trap, which breaks down to 13% and 18% for the pink and white chromotypes, respectively. This agrees well with the modeled 30%–35% relative abundance of *G. ruber* in the nGoM from Lombard et al. (2011), as well as plankton tow and surface sediments throughout the Caribbean Sea, which indicate that *G. ruber* comprises about half of the planktic foraminiferal assemblage (Schmuker & Schiebel, 2002). In the 2008–2014 sediment trap data set the weekly *G. ruber* (white) flux ranges from 0 to 238 tests m^2/day, and *G. ruber* (pink) flux ranges from 0 to 191 tests m^2/day, with a mean flux of 24 and 21 tests m^2/day, for pink and white *G. ruber*, respectively. The two chromotypes of *G. ruber* combined reach their highest relative abundance (50%–75% of the planktic foraminiferal assemblage) from July to September, when overall foraminiferal flux is lowest in the nGoM (Reynolds & Richey, 2016).

The flux time series for the two chromotypes of *G. ruber* covary ($r = 0.76$, $p < 0.01$; Figure 3), suggesting that overall, their production is responding to the same environmental cues. One exception to the covariation in white and pink *G. ruber* flux occurs during 2008–2009, when the flux of white *G. ruber* is anomalously low during all seasons. The average ratio of pink-to-white *G. ruber* is 1.1 (± 0.3) in the sediment trap samples from 2010 to 2014, but the ratio is much higher in 2008 and 2009 (9.2 and 3.3, respectively). This high ratio of pink:white was also observed in plankton tows throughout the Florida Straits and Caribbean Sea (Jentzen et al., 2018) where samples were mostly collected in February/March of 2009. They concluded that the high pink:white ratio was evidence for a basin-wide decrease in the abundance of white *G. ruber* in recent decades, as the pink:white ratio is closer to one in core-top sediments and earlier plankton tow studies. Our time series would suggest that there is inherent interannual variability in the GoM, perhaps due to mesoscale circulation patterns (i.e., loop current eddies). Sporadic propagation of warm-core (i.e., anticyclonic) loop current eddies into the nGoM could account for higher flux of pink, relative to white, *G. ruber*, as assemblages in the Caribbean Sea have higher pink:white (Jentzen et al., 2018). Poore et al. (2013) noted the presence of warm-core loop current eddies at the sediment trap site throughout 2008. These warm-core eddies are characterized by elevated temperature and salinity, and low nutrients and productivity (Biggs, 1992). There is not

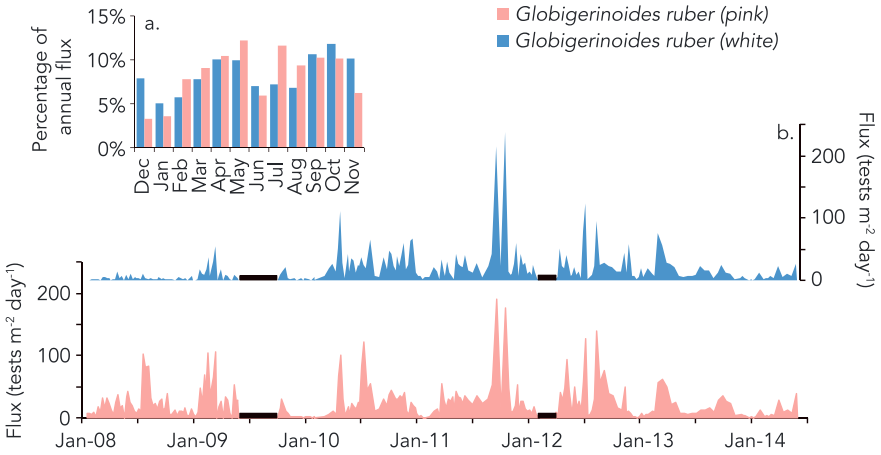

Figure 3. Flux of *G. ruber* in the nGoM. A 6-year time series (2008–2014) of weekly to biweekly flux of *G. ruber* (white) and *G. ruber* (pink). Black bars indicate sampling gaps in 2009 (June–September) and 2012 (February–March). The bar graph (a) shows the percentage of the total flux over the 6-year sampling interval that occurs in each calendar month for both the pink and white chromotypes of *G. ruber*.

an apparent SST or SSS anomaly that would explain the low flux of the white chromotype in 2008–2009 (Poore et al., 2013); however, this interannual variability underscores the value of using data from long-running sediment traps to draw conclusions regarding the seasonal distributions and relative abundance of planktic foraminifera.

Overall, both chromotypes display a similar bimodal distribution with flux peaks in spring and fall, and flux minima in the winter (Figure 3a). Analysis of higher-frequency flux variations from 2010 to 2014 in this sediment trap time series indicates significant lunar periodicity in the flux of both pink and white *G. ruber* (Jonkers et al., 2015). We applied the monthly flux weights for pink and white *G. ruber* to the climatic monthly mean SSTs for the nGoM (HadISST; Rayner et al., 2003), and the resulting flux-weighted annual SST was 25.6 °C and 25.8 °C for white and pink *G. ruber*, respectively. Even though there are clear seasonal variations in *G. ruber* abundance, the mean of *G. ruber* tests (of both chromotypes) exported to the sediments effectively reflect mean-annual SST (observed mean-annual SST is 25.4 °C).

The nGoM flux data set shows that there is effectively no difference in the average relative abundance or seasonal distribution of the two chromotypes of *G. ruber* in the nGoM. This is consistent with a 3-year time series (1997–1999) of pink and white *G. ruber* flux data from the Cariaco Basin sediment trap in the western tropical Atlantic (Tedesco & Thunell, 2003), which also shows no significant difference in the overall abundance of the two chromotypes, and the same bimodal seasonal flux distribution as seen in the nGoM. However, pink and white *G. ruber* start to diverge as you move toward higher latitudes in the North Atlantic. Žarić et al. (2005) concluded from an analysis of global sediment trap data that pink *G. ruber* has a preference for higher SSTs than white *G. ruber*. Tolderlund and Bé, (1971) found that both pink and white *G. ruber* decreased in overall abundance moving from the warm subtropical waters of Bermuda to the colder extratropical North Atlantic Ocean. They concluded that pink *G. ruber* has a lower tolerance for cold water than white *G. ruber*, with pink abundances dropping below average when SSTs are below 24.4 °C, while white *G. ruber* has optimal concentration at temperatures exceeding 21.3 °C (Tolderlund & Bé, 1971). Subsequent sediment trap studies from the Sargasso Sea (32°N; Deuser, 1987; Salmon et al., 2015) and the Azores Current (33°N; Storz et al., 2009) indicate that pink *G. ruber* is much less abundant with <5% of the overall flux of white *G. ruber*. At these midlatitude sites, <4% annual flux occurs in February–May, when average monthly SSTs drop below 19 °C. For this reason, pink *G. ruber* has been interpreted as a summer-weighted species, while white *G. ruber* is typically inferred to be a mean annual SST recorder. We note that nGoM SSTs are warmer than 24 °C for all months except JFM, and therefore, SST has a smaller impact on seasonality of *G. ruber* flux in the nGoM than in the midlatitude North Atlantic Ocean.

Previous studies in the GoM have attributed offsets in the down core geochemistry of pink and white *G. ruber* to differences in their seasonal distribution (Richey et al., 2012; Williams et al., 2010). For example, a

paleoceanographic record spanning the deglaciation from the Orca Basin (nGoM) shows divergences in the elemental and isotopic composition of pink and white *G. ruber* during cold events (e.g., the Oldest and Younger Dryas). During these cooling events, white *G. ruber* indicates significantly colder SSTs than pink *G. ruber*, which the authors attribute to enhanced seasonality (Williams et al., 2010). Given the observation of Tolderlund and Bé (1971) that pink *G. ruber* has a lower tolerance for cold SSTs, it is reasonable to assume that pink *G. ruber* flux was summer weighted in the nGoM during past cold climate regimes. In a late Holocene down core record from the Pigmy Basin, Mg/Ca of co-occurring pink and white *G. ruber* exhibit the same variability (within analytical uncertainty) over the past millennium and suggest no significant differences in the modern seasonal/depth distribution of the chromotypes in the nGoM (Richey et al., 2012). Due to the apparent shift in relative abundance and seasonality of pink and white *G. ruber* between the tropics and the midlatitudes, the findings from the modern nGoM may not necessarily be extrapolated to other regions or cold climate states in the GoM. Under Holocene conditions in the GoM and Caribbean, however, it is reasonable to assume that pink and white *G. ruber* deposited in sediments reflect the same hydrographic conditions.

4.3. Morphological Variability Within *Globigerinoides ruber*

In the nGoM we observe the same morphological diversity in both pink and white *G. ruber*. For this study, we use the criteria described by Wang (2000) to distinguish between the *ss* and *sl* morphotypes of *G. ruber*. Specimens identified as *sl* had a compressed final chamber and included specimens previously identified as *G. elongatus* (D'Orbigny, 1826) and *G. pyramidalis* (Van den Broeck, 1876). Specimens identified as *ss* were characterized by large spherical final chambers situated symmetrically over the suture of the previous two chambers. We note that some studies differentiate *kummerform* (Berger, 1969) specimens, which have diminutive final chambers, but can occur within any of the *G. ruber* morphotypes (e.g., Numberger et al., 2009), and have been attributed to environmental stress. In this sample set we grouped what some might call kummerform specimens into the *sl* morphotype, as these individuals always had compressed and asymmetrical final chambers. Any individual that we determined to be ambiguous (i.e., possessed attributes of both *ss* and *sl* morphotypes), was identified as *intermediate* and was not used for comparisons of geochemistry between the morphotypes.

Pink individuals range from having compressed final chambers of the holotypic *sl G. ruber* to the holotypic *ss G. ruber* (Figure S2, supporting information). This observation is not consistent with the hypothesized divergence between the pink chromotype and the *Globigerinoides conglobatus* lineage (which includes *G. ruber* (*sl*) morphotype; Aurahs et al., 2011). Thirumalai et al. (2014) used samples from the same nGoM sediment trap time series used in this study, along with underlying sediments to demonstrate that there is no significant isotopic difference between co-occurring white *G. ruber sl* and *G. ruber ss*. We include here a parallel data set for *G. ruber* (pink) that shows there is no systematic carbon or oxygen isotopic offset between co-occurring morphotypes of *G. ruber* pink in this sample set (Figure S3, supporting information). Therefore, we did not discriminate between the morphotypes of white or pink *G. ruber* for the paired Mg/Ca-$\delta^{18}O_c$ measurements presented in this study. We did, however, identify every individual that was used for geochemical analysis as *sl*, *ss*, or intermediate, to investigate the overall composition of the *G. ruber* population in the modern water column and to assess seasonal control on morphotype relative abundance. In the nGoM sediment trap time series, pink and white *G. ruber* had identical distributions of morphotypes, with 48% (±14%) of the population (2011–2013) identified as *sl*, 39% (±13%) identified as *ss*, and the remaining 13% of each chromotype was identified as intermediate. While neither morphotype exhibits a strong seasonal preference in white or pink *G. ruber*, the abundance of the *sl* morphotype relative to the *ss* morphotype drops in the late fall/early winter for both chromotypes (Figure S4, supporting information). While this might indicate that the *ss* morphotype has a preference for cooler SSTs compared to *sl*, it is inconsistent with the findings of Antonarakou et al. (2015), which show that reconstructed Mg/Ca-SSTs are systematically higher (warmer) for the *ss* morphotype in Holocene GoM sediments than for the *sl* morphotype.

4.4. Isotopic and Elemental Variability in *Globigerinoides ruber*

Paired elemental (Mg/Ca) and isotopic ($\delta^{18}O$ and $\delta^{13}C$) measurements of both white and pink *G. ruber* were made at weekly-to-monthly resolution for a 3-year interval (2010–2013) of the sediment trap time series (Figure 4). We find no significant difference in the Mg/Ca and $\delta^{18}O$ signals of the two *G. ruber* chromotypes exported to the sediments. White *G. ruber* Mg/Ca varies with the seasonal cycle in SST, ranging from 3.30 to

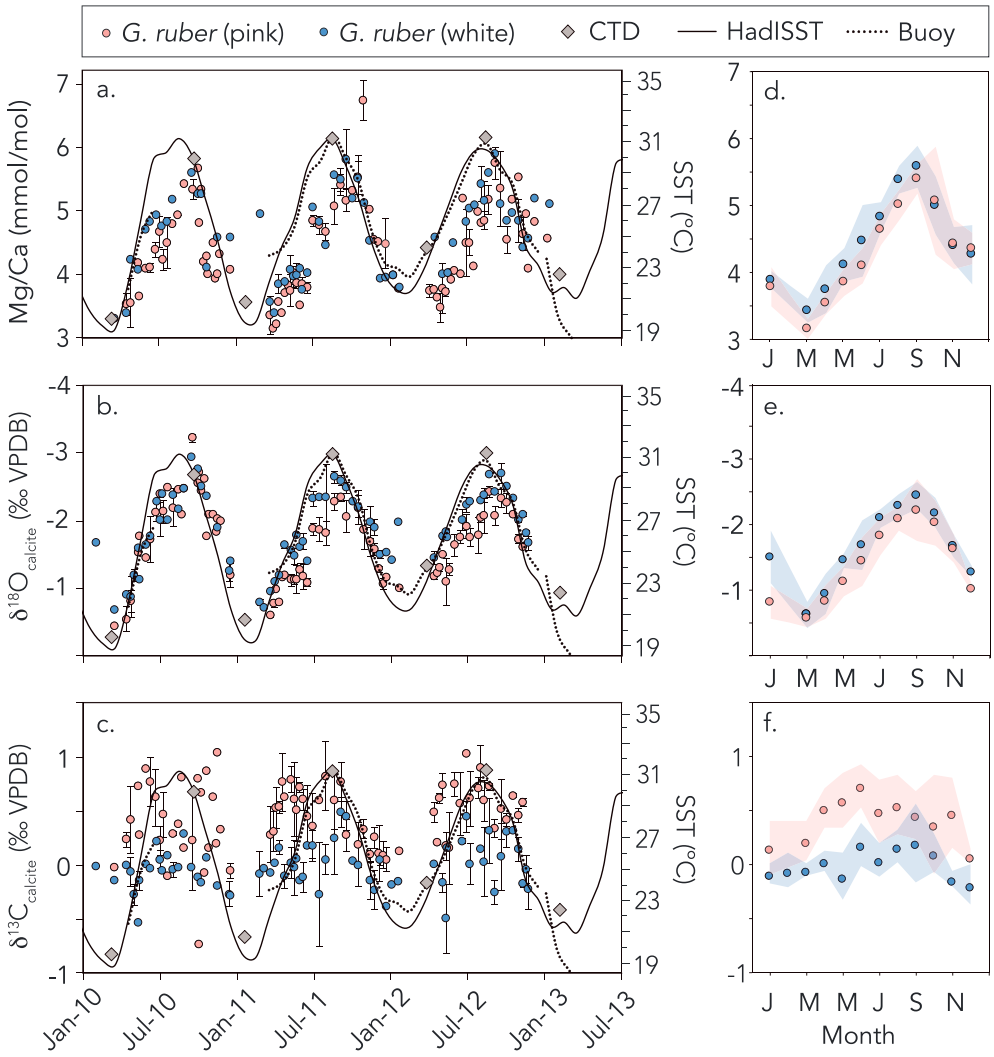

Figure 4. Sediment trap time series of (a) Mg/Ca, (b) $\delta^{18}O_c$, and (c) $\delta^{13}C_c$ of both white (blue circles) and pink (pink circles) *G. ruber* from the nGoM. Vertical error bars represent standard deviations of replicate samples, when available. Solid black line is the HadISST data (Rayner et al., 2003), the dashed line is SST from a local buoy (Green Canyon 205a; http://www.ndbc.noaa.gov), and diamonds are SST observations from CTD casts at the sediment trap site. The composite annual cycle for each parameter was calculated by averaging all values for each calendar month from the 3-year time series in panels d–f. The shaded intervals represent the 1σ range of all measurements for each month.

5.88 mmol/mol, whereas its pink counterpart ranges from 3.15 to 6.73 mmol/mol. The flux-weighted means for white and pink *G. ruber* over the 3-year time series are within 1σ of each other, 4.62 ($\pm$0.43) mmol/mol and 4.41 ($\pm$0.49) mmol/mol, respectively. The $\delta^{18}O_c$ of *G. ruber* varies between $-$3.03% and $-$0.24‰ (pink) and $-$2.75% and $-$0.48‰ (white). The flux-weighted $\delta^{18}O_c$ is $-$1.47‰ (white *G. ruber*) and $-$ 1.53‰ (pink *G. ruber*). The Mg/Ca and $\delta^{18}O$ distributions of the pink and white chromotypes of *G. ruber* are not systematically offset from each other, as shown in the histograms in Figure 5 (two-sample *t* tests fail to reject the null hypothesis at $p < 0.05$). The same is true for paired measurements of Mg/Ca from a 6-year sediment trap time series in the Sargasso Sea (Anand et al., 2003), where the mean Mg/Ca of the two chromotypes is 3.92 and 3.95 mmol/mol, for pink and white *G. ruber*, respectively. This implies that in oceanographic settings where neither pink and white *G. ruber* is close to the limits of their temperature or salinity tolerance, the geochemistry of the two chromotypes could be used interchangeably in down core paleoceanographic reconstructions, as has been done when foraminiferal abundance is limited (Lea et al., 2003).

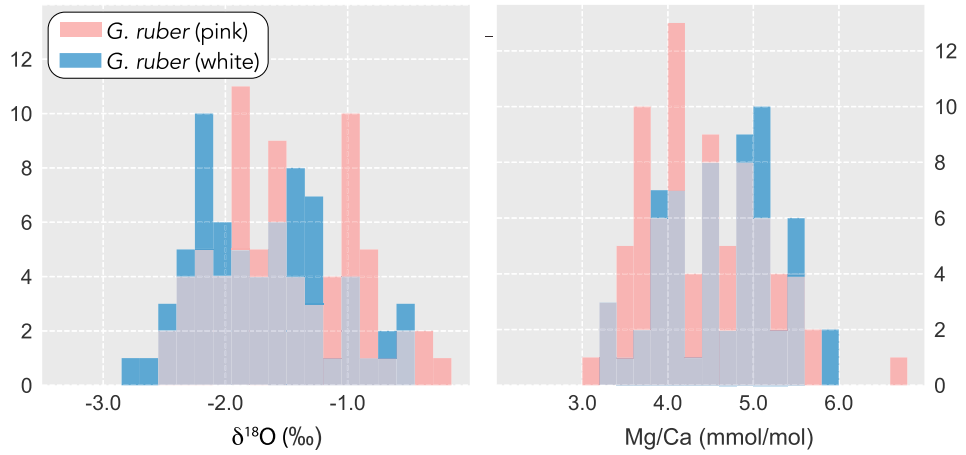

Figure 5. Histograms showing distributions of $\delta^{18}O_c$ and Mg/Ca measurements for *G. ruber* white and *G. ruber* pink from the 2010–2013 sediment trap time series.

The $\delta^{13}C_c$ of pink and white *G. ruber* exhibits modest seasonality (Figure 4f), with a more pronounced summer increase in pink *G. ruber*. *Globigerinoides ruber* (pink) has systematically more enriched $\delta^{13}C$ than *G. ruber* (white), with a mean $\delta^{13}C_c$ of 0.45‰ (±0.31‰, 1σ). *Globigerinoides ruber* (white) has a mean $\delta^{13}C_c$ of −0.01‰ (±0.21‰, 1σ). This average 0.4‰ offset between the carbon isotopic composition of the two chromotypes is also observed in marine sediments (Figure 5c; Elderfield et al., 2002; Richey et al., 2012). Since each of these isotopic measurements was made on an aliquot containing six to eight individual foraminifera ranging from 212 to 425 μm in size, it is likely that large intersample variability can be attributed to variations in the mean test size of samples. A previous study showed that the $\delta^{13}C_c$ of both pink and white *G. ruber* increased by ~0.8‰ between the 212- and 250-μm size fraction and the 355–425-μm size fraction in core-top samples (Richey et al., 2012). We have limited measurements of the $\delta^{13}C$ of dissolved inorganic carbon ($\delta^{13}C_{DIC}$) at our study site (n = 9), where $\delta^{13}C_{DIC}$ in the surface mixed layer varies between 0.6% and 0.7‰ in winter (JFM) and 0.3%–0.5‰ in summer (JAS). This seasonal pattern of $\delta^{13}C_{DIC}$ is consistent with a peak in primary productivity in winter (Muller-Karger et al., 2015), but the overall impact of $\delta^{13}C_{DIC}$ variability is smaller than the influence of test size. Therefore, down core studies using $\delta^{13}C$ of *G. ruber* should take care when interpreting $\delta^{13}C$ variations.

4.5. Foraminiferal Size

Previous studies have demonstrated that foraminiferal isotopic and trace element geochemistry can vary as a function of test size (Anand et al., 2003; Bijma et al., 1998; Elderfield et al., 2002; Friedrich et al., 2012; Richey et al., 2012; Sarkar et al., 1990). An increase in $\delta^{13}C$ with increasing test size is observed in both spinose and nonspinose planktic foraminifera (Berger et al., 1978; Curry & Matthews, 1981; Elderfield et al., 2002; Oppo & Fairbanks, 1989; Ravelo & Fairbanks, 1995) and has been attributed to decreasing metabolic rate with ontogeny (Berger et al., 1978), and enrichment of $\delta^{13}C$due to increasing symbiont photosynthesis in symbiont-bearing species (Bijma et al., 1998; Oppo & Fairbanks, 1989; Spero et al., 1991; Spero & DeNiro, 1987; Spero & Lea, 1993; Spero & Williams, 1988).

The relationship between test size and Mg/Ca is more variable, with some studies showing an increase in Mg/Ca with increasing size (Elderfield et al., 2002; Richey et al., 2012), while others show the opposite relationship (Friedrich et al., 2012). Here we address the question of whether the observed increase in Mg/Ca with increasing test size in pink and white *G. ruber* from nGoM core-top sediments (Richey et al., 2012) can be explained by the depth or seasonal distribution of test sizes. We examined the relationship between test size and Mg/Ca within a single sediment trap cup from a 2-week interval with particularly high flux collected in September 2011. Three aliquots of 100 white *G. ruber* were picked, cleaned, and analyzed separately from four size fractions (150–212, 212–250, 250–300, and 300–355 μm). The Mg/Ca of the four size fractions is not statistically distinguishable among the samples. We repeated the experiment with pink *G. ruber* using four size fractions (212–250, 250–300, 300–355, and 355–425 μm) and find no relationship between test size

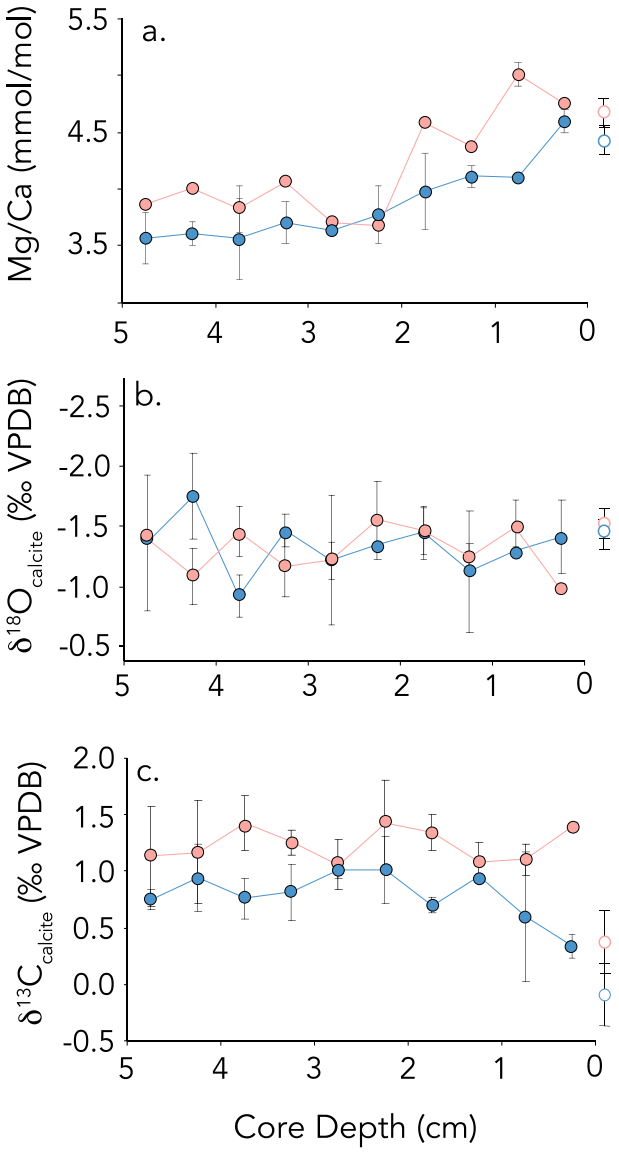

Figure 6. Down core geochemistry for pink *G. ruber* (pink) and white *G. ruber* (blue) from multicores at the nGoM sediment trap site (27.5°N, 90.3°W)––(a) Mg/Ca (mmol/mol) of pink and white *G. ruber*, (b) $\delta^{18}O_{calcite}$ of pink and white *G. ruber*, and (c) $\delta^{13}C_{calcite}$ of pink and white *G. ruber*. Open circles on the right-hand axis of panels a–c indicate flux-weighted means for each of the three measured parameters from the sediment trap time series (2010–2013). Individual data points represent the means of duplicate measurements on separate aliquots of foraminifera from the same sample, and vertical error bars are the standard deviations (1σ).

and Mg/Ca (Figure S5, supporting information). There is not a sufficient number of *G. ruber* tests in any other sediment trap samples to repeat this experiment, but our results illustrate that co-occurring pink and white *G. ruber* of all size fractions calcified at 28.5 °C (± 0.5 °C), all within the upper 50 m of the water column in September.

The increase in Mg/Ca with increasing *G. ruber* test size observed in core-top sediments (Richey et al., 2012) may be explained by the seasonal distribution of test size in the GoM. We look at the monthly size distribution of *G. ruber* in our sediment trap time series (2008–2016) and find that the population is comprised of larger individuals in warmer months (Figure S6, supporting information). Both pink and white *G. ruber* have the largest mean test size in September, when SST in the GoM is warmest. The December–January population of *G. ruber* (white) is >75% composed of the smallest size fraction (150–212 μm). *Globigerinoides ruber* (pink) has an overall larger mean test size than *G. ruber* (white), but it also shows the largest flux of small individuals in winter, with 40% of the population in the <212-μm size fraction. Therefore, the largest and smallest size fractions of *G. ruber* in sediments are likely to be heavily weighted toward summer and winter, respectively. A study of foraminiferal size in global core-top sediments indicated that *G. ruber* reaches maximum test size at the optimum SST of 27.5 °C (Schmidt et al., 2004), consistent with eco-physiological model results that indicate a maximum in *G. ruber* growth rate at 27.5 °C (Lombard et al., 2011). If SST is the primary driver of the seasonal skewing of size fractions in *G. ruber*, it is likely to be more pronounced in the higher latitudes, underscoring the importance of constraining down core analyses to a narrow size range.

4.6. Comparison Between Water Column and Core-Top Foraminiferal Geochemistry

We compare the geochemistry of *G. ruber* in sinking particles to the geochemistry in underlying sediments to determine the degree to which sedimentary foraminifera reflect modern local water column observations and to determine whether there is postdepositional diagenetic alteration of the geochemistry. We analyzed the Mg/Ca, $\delta^{18}O_c$, and $\delta^{13}C$ of pink and white *G. ruber* from the upper 5 cm of a multicore (ca.1940–2010 C.E.) collected from the nGoM sediment trap site in 2013 (Figure 6). The multicore captured the intact sediment-water interface, and an age model was generated based on ^{210}Pb analyses (Richey & Tierney, 2016). The down core Mg/Ca and $\delta^{18}O_c$ values for pink and white *G. ruber* are not significantly different from each other. For both chromotypes, Mg/Ca and $\delta^{18}O_c$ in the upper 2 cm of the sediments are within error of the flux-weighted means based on the 3-year sediment trap time series, with no apparent postdepositional alteration. While the $\delta^{18}O_c$ shows no trend over the past ~70 years of deposition, the Mg/Ca of both pink and white *G. ruber* show a sharp increase in the upper 2.5 cm (after ~1980).

The $\delta^{13}C$ of pink *G. ruber* is more enriched than white *G. ruber* by an average of 0.4‰, equivalent to the $\delta^{13}C$ offset between the chromotypes in the sediment trap (this study) and previously published nGoM core tops (Richey et al., 2012). However, the mean down core $\delta^{13}C$ of both chromotypes is 0.82‰ more enriched than the $\delta^{13}C$ from the sediment trap. The most likely explanation for this offset is the $\delta^{13}C$ Suess effect (Keeling, 1979), in which the $\delta^{13}C$ of dissolved inorganic carbon (DIC) in the surface ocean is decreasing due to the addition of isotopically depleted carbon into the atmosphere via fossil fuel burning. Swart et al. (2010) found that the $\delta^{13}C$ of scleractinian corals in the Atlantic Ocean decreased at a rate of 0.019‰ per year during the 1960–1990 interval. Assuming this rate of change, the 0.82‰ $\delta^{13}C$ depletion in sediment trap samples

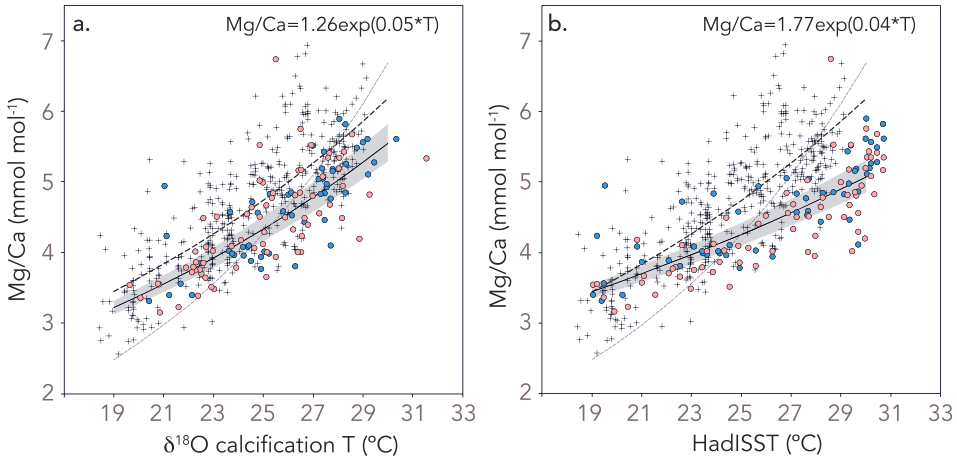

Figure 7. Mg/Ca-temperature relationship for pink and white *G. ruber* in the nGoM sediment trap data set. Mg/Ca is regressed against (a) δ^{18}O-calcification temperature and (b) HadISST. The δ^{18}O-calcification temperature was calculated from paired $\delta^{18}O_c$ data, using the *G. ruber* equation from Mulitza et al. (2003), and assuming a monthly varying $\delta^{18}O_{sw}$. The $\delta^{18}O_{sw}$ was calculated by converting monthly climatological salinity at 20-m water depth (Levitus, 2013) using the regional surface water $^{18}O_{sw}$-salinity equation presented in section 4.1. Gray symbols show the Mg/Ca-T global sediment trap data set for *G. ruber* compiled in Gray et al. (2018). Black dashed line indicates the Mg/Ca-T relationship determined by Gray et al. (2018) [Eq.S1: Mg/Ca = 1.26 exp(0.53T)], and the gray dashed line indicates the Mg/Ca-T relationship determined by Anand et al. (2003) [*G. ruber* (white) equation with fixed exponential constant, Mg/Ca = 0.449*exp(0.09*T)]. The solid black curve in each figure is the exponential Mg/Ca-T relationship determined from the combined pink and white *G. ruber* data set from this study, with the 95% confidence intervals shown in gray shaded intervals.

relative to core-top samples can be accounted for by mixing of middle and late twentieth century material via time averaging and bioturbation. The absence of an apparent trend in the down core $\delta^{13}C$ may be explained by the dominant influence of noise (>1‰ in sediment trap time series) resulting from foraminiferal size differences and/or seasonal changes in $\delta^{13}C_{DIC}$.

4.7. Temperature Sensitivity of Mg/Ca in *Globigerinoides ruber*

Temperature has been established as the primary control on Mg/Ca in planktic foraminifera through laboratory culture (e.g., Allen et al., 2016; Lea et al., 1999), core-top (e.g., Dekens et al., 2002; Lea, 2000), and sediment trap studies (e.g., Anand et al., 2003; McConnell & Thunell, 2005), which converge upon a Mg/Ca-temperature sensitivity of 7%–10%/°C for *G. ruber*. The Sargasso Sea sediment trap calibration study by Anand et al. (2003) is the only one to explicitly publish a Mg/Ca-SST equation for the pink chromotype of *G. ruber*, and they find a significant difference between the Mg/Ca-SST relationships [Mg/Ca = B exp (AT)] of the two chromotypes. In the Anand et al. (2003) equations where the exponential constant is assumed (A = 0.09), the difference in the preexponential constants for the two chromotypes (250–350-μm size fraction) results in an offset of ~2.5 °C in calibrated SST for pink and white *G. ruber* samples with equivalent Mg/Ca. This can lead to ambiguity in the interpretation of contemporaneous down core Mg/Ca records of pink and white *G. ruber* (e.g., Richey et al., 2012; Williams et al., 2010).

We calculate the Mg/Ca-temperature sensitivity for both pink and white *G. ruber* in the nGoM sediment trap data set. Although we are not suggesting that there is a distinct regional Mg/Ca-SST relationship in the nGoM, our data set covers an exceptionally large temperature range relative to other sediment trap studies, and its resolution of the full seasonal cycle makes it ideal for testing whether the pink and white *G. ruber* Mg/Ca-SST relationships are different. Since we do not have continuous in situ temperature observations, we regressed foraminiferal Mg/Ca against two different estimates of calcification temperature: δ^{18}O-calcification temperature and HadISST. The pink and white *G. ruber* data sets do not yield Mg/Ca-SST relationships that are statistically significantly different from one another, regardless of the temperature data set used for calibration (Table S1, supporting information). We show the Mg/Ca-SST regressions for the combined pink and white *G. ruber* data sets using δ^{18}O-calcification temperature (Figure 7a) and HadISST (Figure 7b), resulting in Mg/Ca-temperature sensitivity of 5%/°C

Table 1
List of Equations Used to Solve for SST, SSS, and $\delta^{18}O_{sw}$ in This Study

Equation	Species/region	Equation	Reported statistics	Reference
T	*Globigerinoides ruber*	ln (Mg/Ca) = 0.084*T(°C) + 0.051*SSS − 2.54	$n = 31$, $r^2 = 0.86$, RMSE = 0.12	Tierney et al. (2015)
G	*Globigerinoides ruber*	Mg/Ca = exp(0.60 ± 0.008*T + 0.033 ± 0.022*S − 0.83 ± 0.73*[pH–8] − 1.07 ± 0.80	RSE = 0.50	Gray et al. (2018)
M	*Globigerinoides ruber*	T(°C) = 14.2–4.44($\delta^{18}O_c - \delta^{18}O_c$)	$n = 91$	Mulitza et al. (2003)
HL	*Orbuina universa*, high-light	T(°C) = 14.9(±0.1)–4.80(±0.08)*($\delta^{18}O_c - \delta^{18}O_{sw}$)	$r^2 = 0.96$	Bemis et al. (1998)
LL	*Orbuina universa*, low-light	T(°C) = 16.5 (±0.2)–4.80(±0.16)*($\delta^{18}O_c - \delta^{18}O_{sw}$)	$r^2 = 0.98$	Bemis et al. (1998)
NA	North Atlantic Ocean	$\delta^{18}O_{sw} = 0.55(\pm0.01)*S - 18.98\ (\pm0.16)$	$r^2 = 0.95$	LeGrande and Schmidt (2006)
TA	Tropical Atlantic Ocean	$\delta^{18}O_{sw} = 0.15(\pm0.01)*S - 4.61\ (\pm0.30)$	$r^2 = 0.55$	LeGrande and Schmidt (2006)
FGB	Flower Garden Banks, Gulf of Mexico	$\delta^{18}O_{sw} = 0.19*S - 5.99$	$r^2 = 0.99$	Wagner and Slowey (2011)
Reg	27.5 °N, 90.3 °W, Gulf of Mexico	$\delta^{18}O_{sw} = 0.20(\pm0.03)*S - 6.06(\pm1.06)$	$n = 33$, $r^2 = 0.35$, $p < 0.00001$	this study

[a]Abbreviations in this column are used to refer to these equations throughout this study.

and 4%/°C, respectively. Both regressions indicate that Mg/Ca-temperature sensitivity that is much lower than the 9%/°C of the Anand et al. (2003) equation, which is the most widely used for down core reconstruction of Mg/Ca-SST. Recent sediment trap studies have also found lower Mg/Ca-temperature sensitivity in *G. ruber* than the canonical 9%/°C, including a temperature sensitivity as low as 3%/°C in the Gulf of Tehuantepec (Gibson et al., 2016) and 6%/°C in a global sediment trap data set published by Gray et al. (2018). These discrepancies likely stem from inherent uncertainties in estimating calcification temperature from $\delta^{18}O$ or gridded temperature data sets, as well as secondary controls on foraminiferal Mg/Ca (e.g., salinity and pH).

Although Mg/Ca in planktic foraminifera varies primarily as a function of temperature, early laboratory cultures recognized that both salinity (e.g., Nurnberg et al., 1996; Lea et al., 1999) and carbonate chemistry (e.g., pH and carbonate ion concentration [CO_3^{2-}]) (Lea et al., 1999; Russell et al., 2004) exert secondary controls on Mg/Ca. Some core-top studies have suggested salinity sensitivity as high as 15%–27% in *G. ruber* Mg/Ca (Arbuszewski et al., 2010; Ferguson et al., 2008); however, the majority of culture studies (Kisakürek et al., 2008; Dueñas-Bohórquez et al., 2009; Hönisch et al., 2013), sediment trap (Gray et al., 2018), and reevaluations of those core-top data (Hertzberg & Schmidt, 2013; Hönisch et al., 2013; Khider et al., 2015) suggest that salinity sensitivity is on the order of 3%–6%. Studies evaluating the influence of pH on Mg/Ca in *G. ruber* (Allen et al., 2016; Evans et al., 2016; Gray et al., 2018; Kısakürek et al., 2008) converge on a 5%–10% increase in Mg/Ca per 0.1 unit decrease in pH.

4.8. Comparison of Equations

We do not develop new empirical relationships between *G. ruber* Mg/Ca-$\delta^{18}O_c$ and surface ocean parameters in the nGoM, as in situ observations of carbonate chemistry or salinity are insufficient to quantitatively evaluate pH or salinity sensitivity in this study. In this section we test the performance of a suite of published equations (Table 1) relating hydrographic/geochemical parameters (e.g., temperature, salinity, $\delta^{18}O_{sw}$, pH) and paired Mg/Ca-$\delta^{18}O_c$ of *G. ruber*. The goal is to identify the set of equations that, when applied to the paired Mg/Ca-$\delta^{18}O_c$ data set, most accurately reflects both the mean and variability of these parameters in the upper 50 m of the water column, thus maximizing the accuracy of down core paleoceanographic reconstructions.

Three separate equations are required to derive temperature, salinity, and $\delta^{18}O_{sw}$ from paired Mg/Ca and $\delta^{18}O_c$ measurements in foraminifera: (1) a Mg/Ca-temperature equation, (2) a $\delta^{18}O$-temperature equation, and (3) a $\delta^{18}O_{sw}$-salinity relationship. For the purpose of this exercise, we combined the three years of paired Mg/Ca-$\delta^{18}O_c$ to develop an average annual cycle of mean monthly data for both pink and white *G. ruber*

(Figure 4d and 4e). We then used the PSU Solver algorithm (Thirumalai et al., 2016) to simultaneously solve for the three parameters and their uncertainty envelopes using different combinations of published equations.

We test two different Mg/Ca-SST equations in this section. The first is a multivariate Mg/Ca-SST equation developed by Tierney et al. (2015) from published culture data, which accounts for both the temperature and salinity influence on Mg/Ca. It has a temperature sensitivity of 8%/°C and salinity sensitivity of 5% per psu. The second is a multivariate equation that accounts for the influence of temperature, salinity, and pH on Mg/Ca and was developed by Gray et al. (2018) from a global sediment trap data set. The Gray et al. (2018) equation has a Mg/Ca temperature sensitivity of 6%/°C, a salinity sensitivity of 3% per psu, and a pH sensitivity of −8% per 0.1 pH unit. The Gray et al. (2018) equation requires assumptions about ambient pH, and since we do not have in situ measurements of pH, we developed a mean monthly pH climatology to use in combination with the paired Mg/Ca-$\delta^{18}O_c$ determinations. The details of this calculation are given in the supporting information (Table S2). In brief, we estimated monthly climatologies for two CO_2-system parameters (total alkalinity [A_T] and CO_2 fugacity [fCO_2]) in order to calculate monthly pH. The A_T was derived from local SSS and SST monthly climatological means using the algorithm of Lee et al. (2006), and fCO_2 was obtained from the Surface Ocean CO_2 Atlas (SOCAT; Bakker et al., 2016). The resulting estimate of mean annual surface pH is 8.06, and the annual cycle varies over a 0.21 pH unit range (7.96–8.18). The mean validates well against pH derived from measurements of A_T and total inorganic carbon (TCO_2) in surface water samples ($n = 27$, 0–50-m water depth) spanning the seasonal cycle at the sediment trap site (mean pH: 8.07, pH range: 8.02–8.10). Since the annual range in surface pH estimated from the SOCAT database reflects pH at the air-sea interface, and *G. ruber* calcifies throughout the upper 50 m of the water column, we scaled the annual cycle to reflect the pH range observed in water column measurements (0–50 m) of pH at the sediment trap site (see supporting information).

We evaluate three different $\delta^{18}O_c$-paleotemperature equations to solve for the $\delta^{18}O_{sw}$ from the paired Mg/Ca-$\delta^{18}O_c$ measurements. These include the high-light (HL) and low-light (LL) equations for *Orbulina universa* (Bemis et al., 1998) and the *G. ruber*-specific equation (M) from Mulitza et al. (2003). We compare how the average annual cycle of measured $\delta^{18}O_c$ for pink and white *G. ruber* with the predicted $\delta^{18}O_c$ for depth contours between 0- and 50-m water depth using each of these three paleotemperature equations (Figure S7, supporting information). The LL equation yields predicted $\delta^{18}O_c$ values for the sea surface that are significantly higher than measured $\delta^{18}O_c$ for six months of the year. The *M* equation yields predicted $\delta^{18}O_c$ values that imply *G. ruber* (white and pink) is living between 40–50-m water depth for most of the annual cycle. The HL equation yields predicted $\delta^{18}O_c$ in which the 0–20-m contours overlap with measured $\delta^{18}O_c$ for nine months of the annual cycle.

Finally, in order to convert $\delta^{18}O_{sw}$ to salinity, we test two different linear equations: the north Atlantic (NA) equation from LeGrande and Schmidt (2006), and the new regional mixed-layer equation (Reg) generated in this study (section 4.1). The use of a $\delta^{18}O_{sw}$-salinity transfer function requires an assumption of stationarity in the slope of that relationship through time. We note that the slope of the $\delta^{18}O_{sw}$-salinity relationship likely varied in the GoM under different climate regimes. Notably, there were large inputs of meltwater from the Laurentide Ice Sheet during millennial-scale glacial events and during deglaciation (Flower et al., 2004; Hill et al., 2006; Vetter et al., 2017; Williams et al., 2010). These events almost certainly change the slope of the $\delta^{18}O_{sw}$-salinity relationship by way of a much more $\delta^{18}O$ depleted freshwater endmember than the modern Mississippi River water.

With the 12 possible combinations of the aforementioned equations, we use PSU Solver (Thirumalai et al., 2016) to simultaneously solve for SST, SSS, and $\delta^{18}O_{sw}$ from paired Mg/Ca and $\delta^{18}O_c$ measurements in *G. ruber* (white) from the 2010–2013 sediment trap samples. We summarize the results in Table 2, where the means and annual ranges (monthly maximum minus monthly minimum) of each calculated parameter from the average annual cycle of all paired data in the 3-year sediment trap time series. In order to assess the accuracy of each combination of equations, we calculated the offset ($\Delta\delta^{18}O_{sw}$, ΔSST, and ΔSSS) of the foraminiferal geochemistry-derived value from the mean value of observations in the upper 50 m of the water column for each parameter. A root sum square (RSS) value was then calculated from these three Δ values for each combination of equations, for the purpose of ranking the overall accuracy of each combination, and is ordered from lowest RSS to highest in Table 2.

Table 2
Comparison of $\delta^{18}O_c$-Mg/Ca-Derived and Observed $\delta^{18}O_{sw}$, SST, and SSS for White G. ruber

	Observations	$\delta^{18}O_{sw}$[a]	SST[b]	SSS[c]				
	mean	1.13	24.8	36.2				
	annual range	0.53	7.6	1.3				
Equations		**$\delta^{18}O_{sw}$[d]**	**SST[e]**	**SSS[f]**	**$\Delta\delta^{18}O_{sw}$[g]**	**ΔSST[h]**	**ΔSSS[i]**	**RSS[j]**
G-M-NA	mean	0.78	23.9	35.9	0.35	0.9	0.2	0.96
	range	0.44	6.4	0.8				
T-M-NA	mean	1.20	25.8	36.7	0.07	1.0	0.5	1.08
	range	0.40	5.4	0.7				
G-HL-NA	mean	0.52	24.2	35.5	0.61	0.6	0.7	1.08
	range	0.43	6.5	0.8				
T-M-Reg	mean	1.23	25.9	36.5	0.10	1.1	0.3	1.14
	range	0.31	5.8	1.5				
T-HL-NA	mean	0.92	26.1	36.2	0.21	1.3	0.0	1.29
	range	0.45	5.5	0.8				
G-LL-NA	mean	0.25	25.5	35.5	0.88	0.7	0.7	1.30
	range	0.41	6.5	0.8				
G-HL-Reg	mean	0.91	25.1	34.9	0.22	0.3	1.3	1.35
	range	0.32	6.5	1.6				
G-M-Reg	mean	0.91	24.5	34.9	0.22	0.3	1.3	1.36
	range	0.32	6.5	1.6				
T-LL-NA	mean	0.64	26.4	35.7	0.49	1.6	0.5	1.73
	range	0.47	5.5	0.9				
T-HL-Reg	mean	1.02	26.6	35.4	0.11	1.8	0.8	1.93
	range	0.34	6.0	1.7				
T-LL-Reg	mean	0.81	27.2	34.4	0.32	2.4	1.8	3.00
	range	0.35	6.0	1.7				
G-LL-Reg	mean	0.50	25.6	32.8	0.63	1.4	3.4	3.70
	range	0.32	6.7	1.6				

[a]Mean and range of all $\delta^{18}O_{sw}$ measurements from 0- to 50-m water samples collected at the sediment trap site (2008–2017). [b]Climatic mean annual integrated 0–50-m temperature data from WOA13 (27.5°N, 90.5°W; Locarnini et al., 2013). [c]Mean and range of all salinity observations from CTD casts of the upper 50 m at the sediment trap site (2008–2017). [d]$\delta^{18}O_{sw}$ (‰ VSMOW) calculated from paired $\delta^{18}O_c$ and Mg/Ca in *G. ruber* (white) from the 2008–2014 sediment trap samples. [e]SST (°C) calculated from paired $\delta^{18}O_c$ and Mg/Ca in *G. ruber* (white) from the 2008–2014 sediment trap samples. [f]SSS (psu) calculated from paired $\delta^{18}O_c$ and Mg/Ca in *G. ruber* (white) from the 2008–2014 sediment trap samples. [g]$\Delta\delta^{18}O_{sw}$ is the absolute value of the difference between the mean of derived $\delta^{18}O_{sw}$ and the mean of observed $\delta^{18}O_{sw}$. [h]ΔSST is the absolute value of the difference between the mean of derived SST and the mean of observed SST. [i]ΔSSS is the absolute value of the difference between the mean of derived SSS and the mean of observed SSS. [j]Root sum square of $\Delta\delta^{18}O_{sw}$, ΔSST, and ΔSSS for each combination of equations.

This method of ranking the combinations of equations is designed to test which combination of equations maximizes the accuracy in capturing mean annual conditions of all three parameters. It does not account for how well the calculated parameters match the amplitude of the annual cycle. The two multivariate equations used here result in very similar means and ranges in the sediment trap data set (Figure 8), despite the fact that they prescribe different temperature and salinity sensitivities, and only one equation (Gray et al., 2018) factors in the seasonal variation in pH. SST and pH are anticorrelated in the nGoM seasonal cycle and therefore, when combined, their annual cycle has the same influence on the sign of Mg/Ca change. The collinearity in the two parameters is also an issue in the global sediment trap calibration data set (Gray et al., 2018), resulting in unresolved uncertainty in their relative influence on Mg/Ca.

All combinations of equations result in mean annual SST estimates that are within uncertainty (2σ) of observations except for (T-LL-Reg and T-HL-Reg). All combinations result in salinity estimates that are within uncertainty (2σ) of observations except for three (G-HL-Reg and T-LL-Reg and G-LL-NA), and only half of the combinations of equations result in mean annual $\delta^{18}O_{sw}$ within uncertainty (2σ) of water column observations. Despite the accuracy with which most combinations of equations capture the mean annual SST of the upper 50 m of the water column, none of the equations capture the full range of the seasonal cycle in 0–50-m temperature from WOA13 (Locarnini et al., 2013). This implies that some uncertainties remain in the relative sensitivity of foraminiferal Mg/Ca to temperature, salinity, and pH or in the slope between the

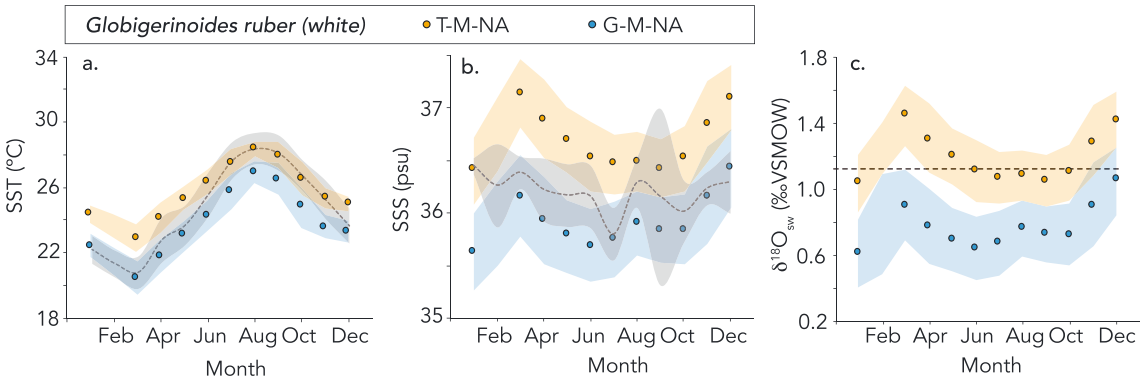

Figure 8. Annual cycle in (a) SST, (b) SSS, and (c) $\delta^{18}O_{sw}$ calculated with PSU Solver (Thirumalai et al., 2016) with the T-M-NA (orange) and G-M-NA (blue) combination of equations applied to paired Mg/Ca and $\delta^{18}O_c$ for *G. ruber* (white). Shaded area represents 1σ uncertainty range. The dashed line in panel a shows the climatological integrated 0–50-m temperature from WOA13 (27.5°N, 90.5°W), with the gray shading showing the 1σ uncertainty range. The dashed line in panel b shows the average 0–50-m salinity observations for each month from CTD casts at the sediment trap site, with the shaded region representing the 1σ uncertainty range. The dashed line in panel c shows the mean measured $\delta^{18}O_{sw}$ from the upper 50 m of the water column from water samples collected 2008–2016.

$\delta^{18}O_{sw}$ and surface-salinity over the annual cycle. The two combinations of equations that have the lowest RSS (i.e., they most accurately reflect the combined temperature, salinity, and $\delta^{18}O_{sw}$ of the upper 50 m of the water column) are T-M-NA and G-M-NA. The annual cycles in SST, SSS, and $\delta^{18}O_{sw}$ derived from these two combinations of equations are shown in Figure 8, with the observational data for reference.

4.9. Implications for Paleoceanographic Reconstruction

As independent proxies for salinity (e.g., Wit et al., 2013) and the carbonate chemistry (e.g., Sosdian et al., 2018) of the ocean become more available in the paleoceanographic record, so will our ability to better constrain SST estimates based on foraminiferal Mg/Ca. We test the impact of accounting for both salinity and pH change in our multicore from the nGoM, which is able to resolve the twentieth century trend due to rapid sediment accumulation rates. In order to look at the impact of twentieth century pH changes on Mg/Ca using the Gray et al. (2018) equation, we estimated surface pH change over the twentieth century in the nGoM using the atmospheric CO_2 data from Mauna Loa Observatory (Keeling et al., 2001) (http://scrippsco2.ucsd.edu/assets/data/atmospheric/merged_ice_core_mlo_spo/merged_ice_core_yearly.csv). We used the climatic mean annual SSS, SST and A_T in the nGoM, along with the pCO_2 data to estimate surface ocean pH for the years sampled in according to our age model (Tables S3 and S4, supporting information). The result is a 0.08 decrease in mean annual surface ocean pH (8.13 to 8.05) from 1942 to 2011, driven by the anthropogenic input of CO_2 into the atmosphere.

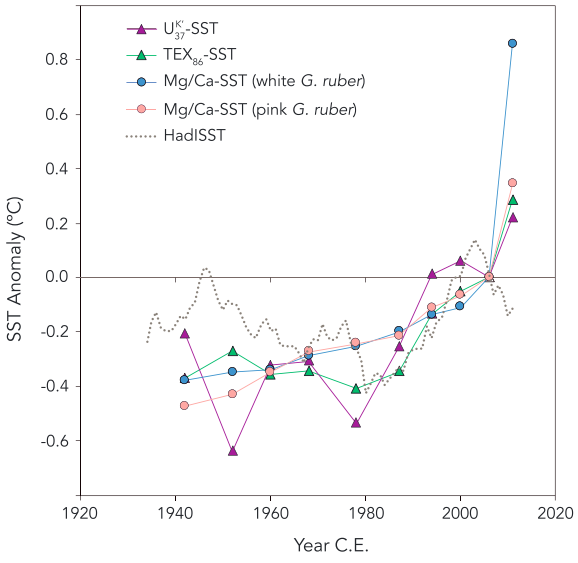

Figure 9. Multiproxy comparison of reconstructed SST anomaly (°C) relative to the 0.5–1.0-cm sample in an nGoM multicore that spans the second half of the twentieth century. TEX_{86}-SST (green triangle), $U^{K'}_{37}$-SST (purple triangle), and Mg/Ca-SST from pink (pink circles) and white (blue circles) *G. ruber* are shown. Gray dashed line shows the decadally filtered mean annual HadISST (Rayner et al., 2003). TEX_{86} and $U^{K'}_{37}$-SST were published in Richey and Tierney (2016). *Globigerinoides ruber* pink and white Mg/Ca was converted to SST using the multivariate equation of Gray et al. (2018) that accounts for temperature, salinity, and pH influence on foraminiferal Mg/Ca.

When we prescribe the calculated pH for the depth intervals in the multicore, and solve for SST using the paired Mg/Ca-$\delta^{18}O$ (Tables S3 and S4, supporting information), we get an increasing temperature trend from Mg/Ca-$\delta^{18}O$ that is equivalent to 0.31 °C from 1950 to 2000 for *G. ruber* (white), 0.37 °C for *G. ruber* pink, both of which are consistent with the warming trend recorded by $U^{K'}_{37}$ and TEX_{86} (Richey & Tierney, 2016) in the same sediment cores (0.36 °C and 0.25 °C, respectively; Figure 9). If we calculate SST warming using an equation that only accounts for temperature and salinity influence on Mg/Ca (T-HL-NA), we get a 1.9 °C warming from 1950 to 2000, whereas using the Anand et al. (2003) equation results in a 1.4 °C warming (4 times the warming estimated from other proxies). The impact of pH on Mg/Ca is less important during the

preindustrial Holocene, when pH was unlikely to have changed significantly. However, oceanic carbonate chemistry changes of the magnitude estimated on glacial-interglacial (Martínez-Botí et al., 2015) and tectonic timescales (Foster & Rohling, 2013) will impact the magnitude of inferred temperature change from foraminiferal Mg/Ca. Ultimately, our analysis indicates that structural uncertainties aside, Mg/Ca-temperature equations considering the effect of salinity and pH along with regionally developed $\delta^{18}O_{sw}$-salinity relationships are most optimal for down core reconstruction.

5. Summary

We use a long-running sediment trap time series in the northern Gulf of Mexico to evaluate the morphometrics, seasonal flux, and geochemistry (Mg/Ca, $\delta^{18}O$, and $\delta^{13}C$) of the white and pink chromotypes of *Globigerinoides ruber***.** Comparison of the two chromotypes indicates that there is no discernable difference between the seasonal flux, Mg/Ca or $\delta^{18}O$ of pink and white *G. ruber*. There is, however, a systematic offset in $\delta^{13}C$ between the two chromotypes, such that pink *G. ruber* is always enriched in $\delta^{13}C$ by ~0.4‰ relative to white *G. ruber*. The flux-weighted mean Mg/Ca and $\delta^{18}O$ of both chromotypes reflects mean annual sea surface hydrography in the nGoM, with flux peaks in the spring and fall, and the lowest flux in winter. Flux-weighted mean Mg/Ca from the 3-year sediment trap time series is 4.62 (±0.43) mmol/mol and 4.41 (±0.49) mmol/mol for white and pink *G. ruber*, respectively; both are within 1σ of their respective core-top Mg/Ca determinations of 4.60 (±0.10) and 4.75 (±0.12) mmol/mol, implying no significant postdepositional alteration of the geochemistry at the sediment-water interface (1,200-m water depth).

We make a new observation regarding the taxonomic relationships between morphotypes of *G. ruber*—the same distribution of *ss* and *sl* morphologies is found in both the pink and white chromotypes of *G. ruber* in the nGoM, in contrast to previous studies that have noted that the pink chromotype is genetically and morphometrically related to the *ss* morphotype of *G. ruber* (white). Furthermore, the oxygen and carbon isotopic composition of the two morphotypes within the pink chromotype are indistinguishable in samples where they are co-occurring. This suggests that there is no difference in the depth habitat or biological fractionation between the morphotypes in the modern nGoM, as was found in a previous study of the white chromotype of *G. ruber* (Thirumalai et al., 2014).

Finally, we evaluated the different combinations of equations for reconstructing SST, SSS, and $\delta^{18}O_{sw}$ from paired Mg/Ca- $\delta^{18}O_c$ measurements in down core paleoceanographic studies from the GoM, including a new regional $\delta^{18}O_{sw}$-salinity relationship for surface mixed layer in the nGoM ($\delta^{18}O_{sw} = 0.19\ (\pm 0.04) * S - 5.08\ (\pm 1.51)$. While the two multivariate Mg/Ca-SST equations we used (Gray et al., 2018; Tierney et al., 2015) both do reasonably well capturing the mean SST, SSS, and $\delta^{18}O_{sw}$ from the sediment trap time series, all combinations of equations fail to capture the full amplitude of the seasonal SST cycle. This suggests that there are still uncertainties in the relative sensitivity of Mg/Ca to temperature, salinity, and pH or the consistency in the slope between $\delta^{18}O_{sw}$ and salinity. When the influence of decreasing ocean pH over the twentieth century is accounted for, *G. ruber* Mg/Ca-SST estimates of surface warming from 1950 to 2000 are in agreement with observational data, as well as TEX_{86} and $U^{K'}_{37}$-SST estimates from the same cores. Taken together, our results refine and further establish the excellent utility of both chromotypes of *G. ruber* as reliable indicators of past ocean and climate variability.

Acknowledgments
We would like to dedicate this work to our colleague and collaborator, Robert Thunell, who has been supportive of the this sediment trap project over the past decade. His expertise and dedication to better understanding paleoceanographic proxies though modern observation is indispensable to the field of paleoceanography. We thank Eric Tappa and the LUMCON crew of the RV *Pelican* for their expert recovery and deployment of the sediment trap mooring since 2008. Thanks to Jennifer Flannery and Cole Spencer for laboratory preparation of samples and geochemical analysis. We thank W. R. Gray, R. Z. Poore, and an anonymous reviewer for their constructive comments on this manuscript. This research was supported by the USGS Land Change Science Program. Any use of trade, firm, or product names is for descriptive purposes only and does not imply endorsement by the U.S. Government. All new data presented in this study can be accessed on PANGAEA (Richey et al., 2019), https://doi.pangaea.de/10.1594/PANGAEA.897517.

References

Allen, K. A., Hönisch, B., Eggins, S. M., Haynes, L. L., Rosenthal, Y., & Yu, J. (2016). Trace element proxies for surface ocean conditions: A synthesis of culture calibrations with planktic foraminifera. *Geochimica et Cosmochimica Acta*, *193*, 197–221. https://doi.org/10.1016/j.gca.2016.08.015

Anand, P., Elderfield, H., & Conte, M. H. (2003). Calibration of Mg/Ca thermometry in planktonic foraminifera from a sediment trap time series. *Paleoceanography*, *18*(2), 1050. https://doi.org/10.1029/2002PA000846

Antonarakou, A., Kontakiotis, G., Mortyn, P. G., Drinia, H., Sprovieri, M., Besiou, E., & Tripsanas, E. (2015). Biotic and geochemical ($\delta^{18}O$, $\delta^{13}C$, Mg/Ca, Ba/Ca) responses of *Globigerinoides ruber* morphotypes to upper water column variations during the last deglaciation, Gulf of Mexico. *Geochimica et Cosmochimica Acta*, *170*, 69–93. https://doi.org/10.1016/j.gca.2015.08.003

Arbuszewski, J., deMenocal, P., Kaplan, A., & Farmer, E. C. (2010). On the fidelity of shell-derived $\delta^{18}O$ seawater estimates. *Earth and Planetary Science Letters*, *300*(3–4), 185–196. https://doi.org/10.1016/j.epsl.2010.10.035

Aurahs, R., Grimm, G. W., Hemleben, V., Hemleben, C., & Kucera, M. (2009). Geographical distribution of cryptic genetic types in the planktonic foraminifer *Globigerinoides ruber*. *Molecular Ecology*, *18*(8), 1692–1706. https://doi.org/10.1111/j.1365-294X.2009.04136.x

Aurahs, R., Treis, Y., Darling, K., & Kucera, M. (2011). A revised taxonomic and phylogenetic concept for the planktonic foraminifer species *Globigerinoides ruber* based on molecular and morphometric evidence. *Marine Micropaleontology*, *79*(1–2), 1–14. https://doi.org/10.1016/j.marmicro.2010.12.001

Bakker, D. C. E., Pfeil, B., Landa, C. S., Metzl, N., O'Brien, K. M., Olsen, A., Smith, K., et al. (2016). A multi-decade record of high quality fCO_2 data in version 3 of the Surface Ocean CO2 Atlas (SOCAT). *Earth System Science Data*, *8*(2), 383–413. https://doi.org/10.5194/essd-8-383-2016

Balmaseda, M. A., Mogensen, K., & Weaver, A. T. (2013). Evaluation of the ECMWF ocean reanalysis system ORAS4. *Quarterly Journal of the Royal Meteorological Society*, *139*(674), 1132–1161. https://doi.org/10.1002/qj.2063

Barker, S., Greaves, M., & Elderfield, H. (2003). A study of cleaning procedures used for foraminiferal Mg/Ca paleothermometry. *Geochemistry, Geophysics, Geosystems*, *4*(9), 8407. https://doi.org/10.1029/2003GC000559

Bé, A. W. H., & Tolderlund, D. S. (1971). In B. M. Funnell & W. R. Riedel (Eds.), *6. Distribution and ecology of living planktonic foraminifera in surface waters of the Atlantic and Indian oceans, in: Micropaleontology of oceans* (pp. 105–149). London, UK: Cambridge University Press.

Bemis, B. E., Spero, H. J., Bijma, J., & Lea, D. W. (1998). Reevaluation of the oxygen isotopic composition of planktonic foraminifera: Experimental results and revised paleotemperature equations. *Paleoceanography*, *13*(2), 150–160. https://doi.org/10.1029/98PA00070

Berger, W. H. (1969). Kummerform foraminifera as clues to oceanic environments. *The American Association of Petroleum Geologists*, *53*, 706.

Berger, W. H., Killingley, J. S., & Vincent, E. (1978). Stable isotopes in deep-sea carbonates: Box core ERDC-92, west equatorial Pacific. *Oceanologica Acta*, *1*, 203–216.

Bhattacharjee, D., Sharma, C., & Bhadury, P. (2013). Chromotypes of *Globigerinoides ruber* in surface sediments from the north-western coast of the Bay of Bengal. *Marine Biodiversity Records*, *6*. https://doi.org/10.1017/S1755267213001097

Biggs, D. C. (1992). Nutrients, plankton, and productivity in a warm-core ring in the western Gulf of Mexico. *Journal of Geophysical Research*, *97*(C2), 2143–2154. https://doi.org/10.1029/90JC02020

Bijma, J., Hemleben, C., Huber, B. T., Erlenkeuser, H., & Kroon, D. (1998). Experimental determination of the ontogenetic stable isotope variability in two morphotypes of *Globigerinella siphonifera* (d'Orbigny). *Marine Micropaleontology*, *35*(3-4), 141–160. https://doi.org/10.1016/S0377-8398(98)00017-6

Boyle, E. A. (1981). Cadmium, zinc, copper, and barium in foraminifera tests. *Earth and Planetary Science Letters*, *53*(1), 11–35. https://doi.org/10.1016/0012-821X(81)90022-4

Boyle, E. A., & Keigwin, L. D. (1985). Comparison of Atlantic and Pacific paleochemical records for the last 215,000 years: Changes in deep ocean circulation and chemical inventories. *Earth and Planetary Science Letters*, *76*(1-2), 135–150. https://doi.org/10.1016/0012-821X(85)90154-2

Conroy, J. L., Thompson, D. M., Cobb, K. M., Noone, D., Rea, S., & Legrande, A. N. (2017). Spatiotemporal variability in the $\delta^{18}O$-salinity relationship of seawater across the tropical Pacific Ocean. *Paleoceanography*, *32*, 484–497. https://doi.org/10.1002/2016PA003073

Coplen, T. B., & Kendall, C. (2000). *Stable hydrogen and oxygen isotope ratios for selected site of the U.S. Geological Survey's NASQAN and benchmark surface-water networks, U.S. Geological Survey Open-File Report 00-160* (p. 424). Reston: U.S. Geological Survey.

Curry, W. B., & Matthews, R. K. (1981). Equilibrium ^{18}O fractionation in small size fraction planktic foraminifera: Evidence from recent Indian Ocean sediments. *Marine Micropaleontology*, *6*, 327–337.

Dekens, P. S., Lea, D. W., Pak, D. K., & Spero, H. J. (2002). Core top calibration of Mg/Ca in tropical foraminifera: Refining paleotemperature estimation. *Geochemistry, Geophysics, Geosystems*, *3*(4), 1022. https://doi.org/10.1029/2001GC000200

Deuser, W. G. (1987). Seasonal variations in isotopic composition and deep-water fluxes of the tests of perennially abundant planktonic foraminifera of the Sargasso Sea: Results from sediment-trap collections and their paleoceanographic significance. *Journal of Foraminiferal Research*, *17*(1), 14–27. https://doi.org/10.2113/gsjfr.17.1.14

D'Orbigny, A. D. (1826). Tableau méthodique de la classe des Céphalopodes. *Annales des Sciences Naturelles. Series I*, *7*, 1–277.

Dueñas-Bohórquez, A., da Rocha, R. E., Kuroyanagi, A., Bijma, J., & Reichart, G.-J. (2009). Effect of salinity and seawater calcite saturation state on Mg and Sr incorporation in cultured planktonic foraminifera. *Marine Micropaleontology*, *73*(3–4), 178–189. https://doi.org/10.1016/j.marmicro.2009.09.002

Elderfield, H., Vautravers, M., & Cooper, M. (2002). The relationship between shell size and Mg/Ca, Sr/Ca, $\delta^{18}O$ and $\delta^{13}C$ of species of planktonic foraminifera. *Geochemistry, Geophysics, Geosystems*, *3*(8), 1052. https://doi.org/10.1029/2001GC000194

Evans, D., Wade, B. S., Henehan, M., Erez, J., & Müller, W. (2016). Revisiting carbonate chemistry controls on planktic foraminifera Mg/Ca: Implications for sea surface temperature and hydrology shifts over the Paleocene–Eocene Thermal Maximum and Eocene–Oligocene transition. *Climate of the Past*, *12*(4), 819–835. https://doi.org/10.5194/cp-12-819-2016

Ferguson, J. E., Henderson, G. M., Kucera, M., & Rickaby, R. E. M. (2008). Systematic change of foraminiferal Mg/Ca ratios across a strong salinity gradient. *Earth and Planetary Science Letters*, *265*(1–2), 153–166. https://doi.org/10.1016/j.epsl.2007.10.011

Flower, B. P., Hastings, D. W., Hill, H. W., & Quinn, T. M. (2004). Phasing of deglacial warming and Laurentide Ice Sheet meltwater in the Gulf of Mexico. *Geology*, *32*(7), 597. https://doi.org/10.1130/G20604.1

Foster, G. L., & Rohling, E. J. (2013). Relationship between sea level and climate forcing by CO_2 on geological timescales. *Proceedings of the National Academy of Science*, *110*(4), 1209–1214. https://doi.org/10.1073/pnas.1216073110/-/DCSupplemental

Friedrich, O., Schiebel, R., Wilson, P. A., Weldeab, S., Beer, C. J., Cooper, M. J., & Fiebig, J. (2012). Influence of test size, water depth, and ecology on Mg/Ca, Sr/Ca, $\delta^{18}O$ and $\delta^{13}C$ in nine modern species of planktic foraminifers. *Earth and Planetary Science Letters*, *319–320*, 133–145.

Gibson, K. A., Thunell, R. C., Machain-Castillo, M. L., Fehrenbacher, J., Spero, H. J., Wejnert, K., et al. (2016). Evaluating controls on planktonic foraminiferal geochemistry in the eastern tropical North Pacific. *Earth and Planetary Science Letters*, *452*, 90–103. https://doi.org/10.1016/j.epsl.2016.07.039

Gray, W. R., Weldeab, S., Lea, D. W., Rosenthal, Y., Gruber, N., Donner, B., & Fischer, G. (2018). The effects of temperature, salinity, and the carbonate system on Mg/Ca in *Globigerinoides ruber* (white): A global sediment trap calibration. *Earth and Planetary Science Letters*, *482*, 607–620. https://doi.org/10.1016/j.epsl.2017.11.026

Hathorne, E. C., Gagnon, A., Felis, T., Adkins, J., Asami, R., Boer, W., et al. (2013). Interlaboratory study for coral Sr/Ca and other element/Ca ratio measurements. *Geochemistry, Geophysics, Geosystems*, *14*, 3730–3750. https://doi.org/10.1002/ggge.20230

Hertzberg, J. E., & Schmidt, M. W. (2013). Refining *Globigerinoides ruber* Mg/Ca paleothermometry in the Atlantic Ocean. *Earth and Planetary Science Letters*, *383*, 123–133. https://doi.org/10.1016/j.epsl.2013.09.044

Hill, H. W., Flower, B. P., Quinn, T. M., Hollander, D. J., & Guilderson, T. P. (2006). Laurentide Ice Sheet meltwater and abrupt climate change during the last glaciation. *Paleoceanography*, *21*, PA1006. https://doi.org/10.1029/2005PA001186

Hönisch, B., Allen, K. A., Lea, D. W., Spero, H. J., Eggins, S. M., Arbuszewski, J., et al. (2013). The influence of salinity on Mg/Ca in planktic foraminifers—Evidence from cultures, core-top sediments and complementary $\delta^{18}O$. *Geochimica et Cosmochimica Acta*, *121*, 196–213. https://doi.org/10.1016/j.gca.2013.07.028

Huang, H., Walker, N. D., Hsueh, Y., Chao, Y., & Leben, R. R. (2013). An analysis of loop current frontal eddies in a 1/6° Atlantic Ocean model simulation. *Journal of Physical Oceanography*, *43*(9), 1924–1939. https://doi.org/10.1175/JPO-D-12-0227.1

Ingleby, B., & Huddleston, M. (2007). Quality control of ocean temperature and salinity profiles—Historical and real-time data. *Journal of Marine Systems*, *65*(1–4), 158–175. https://doi.org/10.1016/j.jmarsys.2005.11.019

Jentzen, A., Schönfeld, J., & Schiebel, R. (2018). Assessment of the effect of increasing temperature on the ecology and assemblage structure of modern planktic foraminifer in the Caribbean and surrounding seas. *Journal of Foraminiferal Research*, *48*(3), 251–272.

Jonkers, L., Reynolds, C. E., Richey, J., & Hall, I. R. (2015). Lunar periodicity in the shell flux of planktonic foraminifera in the Gulf of Mexico. *Biogeosciences*, *12*(10), 3061–3070. https://doi.org/10.5194/bg-12-3061-2015

Keeling, C. D. (1979). The Suess effect: ^{13}Carbon-^{14}Carbon interrelations. *Environment International*, *2*(4–6), 229–300. https://doi.org/10.1016/0160-4120(79)90005-9

Keeling, C. D., Piper, S. C., Bacastow, R. B., Wahlen, M., Whorf, T. P., Heimann, M., & Meijer, H. A. (2001). Exchanges of atmospheric CO2 and 13CO2 with the terrestrial biosphere and oceans from 1978 to 2000. I. Global aspects, SIO Reference Series, No. 01-06 (88 pp.). San Diego, CA: Scripps Institution of Oceanography.

Khider, D., Huerta, G., Jackson, C., Stott, L. D., & Emile-Geay, J. (2015). A Bayesian, multivariate calibration for *Globigerinoides ruber* Mg/Ca. *Geochemistry, Geophysics, Geosystems*, *16*, 2916–2932. https://doi.org/10.1002/2015GC005844

Kısakürek, B., Eisenhauer, A., Böhm, F., Garbe-Schönberg, D., & Erez, J. (2008). Controls on shell Mg/Ca and Sr/Ca in cultured planktonic foraminiferan, *Globigerinoides ruber* (white). *Earth and Planetary Science Letters*, *273*(3–4), 260–269. https://doi.org/10.1016/j.epsl.2008.06.026

Lea, D. W. (2000). Climate impact of Late Quaternary equatorial Pacific sea surface temperature variations. *Science*, *289*(5485), 1719–1724. https://doi.org/10.1126/science.289.5485.1719

Lea, D. W., & Boyle, E. A. (1991). Barium in planktonic foraminifera. *Geochimica Cosmochimica Acta*, *55*(11), 3321–3331. https://doi.org/10.1016/0016-7037(91)90491-M

Lea, D. W., Mashiotta, T. A., & Spero, H. J. (1999). Controls on magnesium and strontium uptake in planktonic foraminifera determined by live culturing. *Geochimica Cosmochimica Acta*, *63*(16), 2369–2379. https://doi.org/10.1016/S0016-7037(99)00197-0

Lea, D. W., Pak, D. K., Peterson, L. C., & Hughen, K. A. (2003). Synchroneity of tropical and high-latitude Atlantic temperatures over the Last Glacial Termination. *Science*, *301*(5638), 1361–1364. https://doi.org/10.1126/science.1088470

Lee, K., Tong, L. T., Millero, F. J., Sabine, C. L., Dickson, A. G., Goyet, C., et al. (2006). Global relationships of total alkalinity with salinity and temperature in surface waters of the world's oceans. *Geophysical Research Letters*, *33*, L19605. https://doi.org/10.1029/2006GL027207

Lee, T. N., Leaman, K., Williams, E., Berger, T., & Atkinson, L. (1995). Florida current meanders and gyre formation in the southern Straits of Florida. *Journal of Geophysical Research*, *100*(C5), 8607–8620. https://doi.org/10.1029/94JC02795

LeGrande, A. N., & Schmidt, G. A. (2006). Global gridded data set of the oxygen isotopic composition in seawater. *Geophysical Research Letters*, *33*, L12604. https://doi.org/10.1029/2006GL026011

Levitus, S. (2003). *National Oceanographic Date Center World Ocean Atlas 1994*. Boulder, CO: Climate Data Center. Retrieved from http://www.cdc.noaa.gov

Lindo-Atichati, D., Bringas, F., & Goni, G. (2013). Loop current excursions and ring detachments during 1993–2009. *International Journal of Remote Sensing*, *34*(14), 5042–5053. https://doi.org/10.1080/01431161.2013.787504

Locarnini, R. A., Mishonov, A. V., Antonov, J. I., Boyer, T. P., Garcia, H. E., Baranova, O. K., et al. (2013). World Ocean Atlas 2013, Volume 1: Temperature. In S. Levitus & A. Mishonov (Eds.), *NOAA Atlas NESDIS 73* (40 pp.).

LoDico, J. M., Flower, B. P., & Quinn, T. M. (2006). Subcentennial-scale climatic and hydrologic variability in the Gulf of Mexico during the early Holocene. *Paleoceanography*, *21*, PA3015. https://doi.org/10.1029/2005PA001243

Lombard, F., Labeyrie, L., Michel, E., Bopp, L., Cortijo, E., Retailleau, S., et al. (2011). Modelling planktic foraminifer growth and distribution using an ecophysiological multi-species approach. *Biogeosciences*, *8*(4), 853–873. https://doi.org/10.5194/bg-8-853-2011

Martínez-Botí, M. A., Foster, G. L., Chalk, T. B., Rohling, E. J., Sexton, P. F., Lunt, D. J., et al. (2015). Plio-Pleistocene climate sensitivity evaluated using high-resolution CO_2 records. *Nature*, *518*(7537), 49–54. https://doi.org/10.1038/nature14145

McConnell, M. C., & Thunell, R. C. (2005). Calibration of the planktonic foraminiferal Mg/Ca paleothermometer: Sediment trap results from the Guaymas Basin, Gulf of California. *Paleoceanography*, *20*, PA2016. https://doi.org/10.1029/2004PA001077

Meckler, A. N., Schubert, C. J., Hochuli, P. A., Plessen, B., Birgel, D., Flower, B. P., et al. (2008). Glacial to Holocene terrigenous organic matter input to sediments from Orca Basin, Gulf of Mexico—A combined optical and biomarker approach. *Earth and Planetary Science Letters*, *272*(1–2), 251–263. https://doi.org/10.1016/j.epsl.2008.04.046

Mulitza, S., Boltovskoy, D., Donner, B., Meggers, H., Paul, A., & Wefer, G. (2003). Temperature: $\delta^{18}O$ relationships of planktonic foraminifera collected from surface waters. *Palaeogeography, Palaeoclimatology, Palaeoecology*, *202*(1–2), 143–152. https://doi.org/10.1016/S0031-0182(03)00633-3

Muller-Karger, F. E., Smith, J. P., Werner, S., Chen, R., Roffer, M., Liu, Y., et al. (2015). Natural variability of surface oceanographic conditions in the offshore Gulf of Mexico. *Progress in Oceanography*, *134*, 54–76. https://doi.org/10.1016/j.pocean.2014.12.007

Numberger, L., Hemleben, C., Hoffmann, R., Mackensen, A., Schulz, H., Wunderlich, J.-M., & Kucera, M. (2009). Habitats, abundance patterns and isotopic signals of morphotypes of the planktonic foraminifer *Globigerinoides ruber* (d'Orbigny) in the eastern Mediterranean Sea since the Marine Isotopic Stage 12. *Marine Micropaleontology*, *73*(1–2), 90–104. https://doi.org/10.1016/j.marmicro.2009.07.004

Nurnberg, D., Bijma, J., & Hemleben, C. (1996). Assessing the reliability of magnesium in foraminiferal calcite as a procy for water mass temperatures. *Geochimica et Cosmochimica Acta*, *60*(5), 803–814. https://doi.org/10.1016/0016-7037(95)00446-7

Nürnberg, D., Ziegler, M., Karas, C., Tiedemann, R., & Schmidt, M. W. (2008). Interacting loop current variability and Mississippi River discharge over the past 400 kyr. *Earth and Planetary Science Letters*, *272*(1–2), 278–289. https://doi.org/10.1016/j.epsl.2008.04.051

Oppo, D. W., & Fairbanks, R. G. (1989). Carbon isotope composition of tropical surface water during the past 22,000 years. *Paleoceanography*, *4*(4), 333–351. https://doi.org/10.1029/PA004i004p00333

Poore, R. Z., Tedesco, K. A., & Spear, J. W. (2013). Seasonal flux and assemblage composition of planktic foraminifers from a sediment-trap study in the northern Gulf of Mexico. *Journal of Coastal Research*, *63*, 6–19. https://doi.org/10.2112/SI63-002.1

Ravelo, A. C., & Fairbanks, R. G. (1995). Carbon isotope fractionation in multiple species of planktonic foraminifera from core tops in the tropical Atlantic. *Journal of Foraminiferal Research*, *25*(1), 53–74. https://doi.org/10.2113/gsjfr.25.1.53

Rayner, N. A., Parker, D. E., Horton, E. B., Folland, C. K., Alexander, L. V., Rowell, D. P., et al. (2003). Global analyses of sea surface temperature, sea ice, and night marine air temperature since the late nineteenth century. *Journal of Geophysical Research*, *108*(D14), 4407. https://doi.org/10.1029/2002JD002670

Reynolds, C. E., & Richey, J. N. (2016). Seasonal flux and assemblage composition of planktic foraminifera from the northern Gulf of Mexico, 2008–14: U.S. Geological Survey Open-File Report 2016–1115 (14 p.). https://doi.org/10.3133/ofr20161115

Reynolds, C. E., Richey, J. N., Fehrenbacher, J. S., Rosenheim, B. E., & Spero, H. J. (2018). Environmental controls on the geochemistry of *Globorotalia truncatulinoides* in the Gulf of Mexico: Implications for paleoceanographic reconstructions. *Marine Micropaleontology*, *142*, 92–104. https://doi.org/10.1016/j.marmicro.2018.05.006

Richey, J. N., Hollander, D. J., Flower, B. P., & Eglinton, T. I. (2011). Merging late Holocene molecular organic and foraminiferal-based geochemical records of sea surface temperature in the Gulf of Mexico. *Paleoceanography*, *26*, PA1209. https://doi.org/10.1029/2010PA002000

Richey, J. N., Poore, R. Z., Flower, B. P., & Hollander, D. J. (2012). Ecological controls on the shell geochemistry of pink and white *Globigerinoides ruber* in the northern Gulf of Mexico: Implications for paleoceanographic reconstruction. *Marine Micropaleontology*, *82–83*, 28–37.

Richey, J. N., Poore, R. Z., Flower, B. P., & Quinn, T. M. (2007). 1400 yr multiproxy record of climate variability from the northern Gulf of Mexico. *Geology*, *35*(5), 423. https://doi.org/10.1130/G23507A.1

Richey, J. N., Poore, R. Z., Flower, B. P., Quinn, T. M., & Hollander, D. J. (2009). Regionally coherent Little Ice Age cooling in the Atlantic Warm Pool. *Geophysical Research Letters*, *36*, L21703. https://doi.org/10.1029/2009GL040445

Richey, J. N., Reynolds, C. E., Tappa, E., & Thunell, R. (2014). Weekly resolution particulate flux from a sediment trap in the northern Gulf of Mexico: U.S. Geological Survey Open-File Report 2014-1035 (9 p.). https://doi.org/10.3133/ofr20141035

Richey, J. N., Thirumalai, K., Khider, D., Reynolds, C. E., Partin, J. W., Quinn, T. M. (2019): *Globigerinoides ruber* sediment trap data in the Gulf of Mexico. *PANGAEA*. https://doi.org/10.1594/PANGAEA.897517

Richey, J. N., & Tierney, J. E. (2016). GDGT and alkenone flux in the northern Gulf of Mexico: Implications for the TEX_{86} and $UK^{'}37$ paleothermometers. *Paleoceanography*, *31*, 1547–1561. https://doi.org/10.1002/2016PA003032

Russell, A. D., Hönisch, B., Spero, H. J., & Lea, D. W. (2004). Effects of seawater carbonate ion concentration and temperature on shell U, Mg, and Sr in cultured planktonic foraminifera. *Geochimica et Cosmochimica Acta*, *68*(21), 4347–4361. https://doi.org/10.1016/j.gca.2004.03.013

Sadekov, A., Eggins, S. M., De Deckker, P., & Kroon, D. (2008). Uncertainties in seawater thermometry deriving from intratest and intertest Mg/Ca variability in *Globigerinoides ruber*. *Paleoceanography*, *23*, PA1215. https://doi.org/10.1029/2007PA001452

Salmon, K. H., Anand, P., Sexton, P. F., & Conte, M. (2015). Upper ocean mixing controls the seasonality of planktonic foraminifer fluxes and associated strength of the carbonate pump in the oligotrophic North Atlantic. *Biogeosciences*, *12*(1), 223–235. https://doi.org/10.5194/bg-12-223-2015

Sarkar, A., Ramesh, R., & Bhattacharya, S. K. (1990). Effect of sample pretreatment and size fraction on the $\delta^{18}O$ and $\delta^{13}C$ values of foraminifera in Arabian Sea sediments. *Terra Nova*, *2*(5), 488–493. https://doi.org/10.1111/j.1365-3121.1990.tb00107.x

Schmidt, D. N., Renaud, S., Bollmann, J., Schiebel, R., & Thierstein, H. R. (2004). Size distribution of Holocene planktic foraminifer assemblages: Biogeography, ecology and adaptation. *Marine Micropaleontology*, *50*(3–4), 319–338. https://doi.org/10.1016/S0377-8398(03)00098-7

Schmidt, G. A., Bigg, G. R., & Rohling, E. J. (1999). *Global seawater oxygen-18 database*. New York: NASA Goddard Inst. Of space Sci. Retrieved from http://data.giss.nasa.gov/o18data

Schmuker, B., & Schiebel, R. (2002). Planktic foraminifers and hydrography of the eastern and northern Caribbean Sea. *Marine Micropaleontology*, *46*(3–4), 387–403. https://doi.org/10.1016/S0377-8398(02)00082-8

Schrag, D. P. (1999). Rapid analysis of high-precision Sr/Ca ratios in corals and other marine carbonates. *PaleoceanographicCurrents*, *40*(2), 97–102.

Sosdian, S. M., Greenop, R., Hain, M. P., Foster, G. L., Pearson, P. N., & Lear, C. H. (2018). Constraining the evolution of Neogene ocean carbonate chemistry using the boron isotope pH proxy. *Earth and Planetary Science Letters*, *498*, 362–376.

Spero, H. J., & DeNiro, M. J. (1987). The influence of symbiont photosynthesis on the $\delta^{18}O$ and $\delta^{13}C$ values of planktonic foraminiferal shell calcite. *Symbiosis*, *4*, 213–228.

Spero, H. J., & Lea, D. W. (1993). Intraspecific stable isotope variability in the planktic foraminifera *Globigerinoides sacculifer*: Results from laboratory experiments. *Marine Micropaleontology*, *22*(3), 221–234. https://doi.org/10.1016/0377-8398(93)90045-Y

Spero, H. J., Lerche, I., & Williams, D. F. (1991). Opening the carbon isotope "vital effect"black box: 2. Quantitative model for interpreting foraminiferal carbon isotope data. *Paleoceanography*, *6*(6), 639–655. https://doi.org/10.1029/91PA02022

Spero, H. J., & Williams, D. F. (1988). Extracting environmental information from planktonic foraminiferal $\delta^{13}C$ data. *Nature*, *375*, 717–719.

Steinke, S., Chiu, H.-Y., Yu, P.-S., Shen, C.-C., Löwemark, L., Mii, H.-S., & Chen, M.-T. (2005). Mg/Ca ratios of two *Globigerinoides ruber* (white) morphotypes: Implications for reconstructing past tropical/subtropical surface water conditions. *Geochemistry, Geophysics, Geosystems*, *6*, Q11005. https://doi.org/10.1029/2005GC000926

Storz, D., Schulz, H., Waniek, J. J., Schulz-Bull, D. E., & Kučera, M. (2009). Seasonal and interannual variability of the planktic foraminiferal flux in the vicinity of the Azores Current. *Deep Sea Research Part I: Oceanographic Research Papers*, *56*(1), 107–124. https://doi.org/10.1016/j.dsr.2008.08.009

Swart, P. K., Greer, L., Rosenheim, B. E., Moses, C. S., Waite, A. J., Winter, A., et al. (2010). The ^{13}C Suess effect in scleractinian corals mirror changes in the anthropogenic CO_2 inventory of the surface oceans. *Geophysical Research Letters*, *37*, L05604. https://doi.org/10.1029/2009GL041397

Tedesco, K. A., & Thunell, R. C. (2003). Seasonal and interannual variations in the planktonic foraminiferal flux and assemblage composition in the Cariaco Basin Venezuela. *Journal of Foraminiferal Research*, *33*(3), 192–210. https://doi.org/10.2113/33.3.192

Thirumalai, K., Quinn, T. M., & Marino, G. (2016). Constraining past seawater $\delta^{18}O$ and temperature records developed from foraminiferal geochemistry. *Paleoceanography*, *31*, 1409–1422. https://doi.org/10.1002/2016PA002970

Thirumalai, K., Quinn, T. M., Okumura, Y., Richey, J. N., Partin, J. W., Poore, R. Z., & Moreno-Chamarro, E. (2018). Pronounced centennial-scale Atlantic Ocean climate variability correlated with Western Hemisphere hydroclimate. *Nature Communications*, *9*(1), 392. https://doi.org/10.1038/s41467-018-02846-4

Thirumalai, K., Richey, J. N., Quinn, T. M., & Poore, R. Z. (2014). *Globigerinoides ruber* morphotypes in the Gulf of Mexico: A test of null hypothesis. *Scientific Reports*, *4*, 6018.

Thirumalai, K., Singh, A., & Ramesh, R. (2011). A MATLAB™ code to perform weighted linear regression with (correlated or uncorrelated) errors in bivariate data. *Journal of the Geological Society of India*, *77*(4), 377–380. https://doi.org/10.1007/s12594-011-0044-1

Thompson, P. R., Be, A. W. H., Duplessy, J. C., & Shackleton, N. J. (1979). Disappearance of pink pigmented *Globigerinoides ruber* at 120,000 yr BP in the Indian and Pacific Oceans. *Nature*, *280*(5723), 554–558. https://doi.org/10.1038/280554a0

Tierney, J. E., Pausata, F. S. R., & deMenocal, P. (2015). Deglacial Indian monsoon failure and North Atlantic stadials linked by Indian Ocean surface cooling. *Nature Geoscience*, *9*(1), 46–50.

Tolderlund, D. S., & Bé, A. W. H. (1971). Seasonal distribution of foraminifera in the western North Atlantic. *Micropaleontology*, *17*(3), 297–329. https://doi.org/10.2307/1485143

Van den Broeck, E. (1876). Etude sur les Foraminiferes de la Barbade (Antilles). *Soc. Belge Microsc. An.*, *1*, 55–152.

Venancio, I. M., Belem, A. L., Santos, T. P., Lessa, D. O., Albuquerque, A. L. S., Mulitza, S., et al. (2017). Calcification depths of planktonic foraminifera from the southwestern Atlantic derived from oxygen isotope analyses of sediment trap material. *Marine Micropaleontology*, *136*, 37–50. https://doi.org/10.1016/j.marmicro.2017.08.006

Vetter, L., Spero, H. J., Eggins, S. M., Williams, C., & Flower, B. P. (2017). Oxygen isotope geochemistry of Laurentide ice-sheet meltwater across Termination I. *Quaternary Science Reviews*, *178*, 102–117. https://doi.org/10.1016/j.quascirev.2017.10.007

Vukovich, F. M. (2007). Climatology of ocean features in the Gulf of Mexico using satellite remote sensing data. *Journal of Physical Oceanography*, *37*(3), 689–707. https://doi.org/10.1175/JPO2989.1

Wagner, A. J., & Slowey, N. C. (2011). Oxygen isotopes in seawater from the Texas-Louisiana Shelf. *Bulletin of Marine Science*, *87*(1), 1–12. https://doi.org/10.5343/bms.2010.1004

Walker, N. D., Pilley, C. T., Raghunathan, V. V., D'Sa, E. J., Leben, R. R., Hoffman, N. G., et al. (2011). Impacts of a loop current frontal eddy cyclone and wind forcing on the 2010 Gulf of Mexico oil spill. In Y. Liu, et al. (Eds.), *Monitoring and modeling the Deepwater Horizon oil spill: A record-breaking enterprise, Geophysical Monograph Series* (pp. 103–116). Washington, DC: American Geophysical Union. https://doi.org/10.1029/2011GM001120

Wang, L. (2000). Isotopic signals in two morphotypes of *Globigerinoides ruber* (white) from the South China Sea: Implications for monsoon climate change during the last glacial cycle. *Palaeogeography Palaeoclimatology Palaeoecology*, *161*(3-4), 381–394. https://doi.org/10.1016/S0031-0182(00)00094-8

Williams, C., Flower, B. P., Hastings, D. W., Guilderson, T. P., Quinn, K. A., & Goddard, E. A. (2010). Deglacial abrupt climate change in the Atlantic Warm Pool: A Gulf of Mexico perspective. *Paleoceanography*, *25*, PA4221. https://doi.org/10.1029/2010PA001928

Wit, J. C., de Nooijer, L. J., Wolthers, M., & Reichart, G. J. (2013). A novel salinity proxy based on Na incorporation into foraminiferal calcite. *Biogeosciences*, *10*(10), 6375–6387.

Žarić, S., Donner, B., Fischer, G., Mulitza, S., & Wefer, G. (2005). Sensitivity of planktic foraminifera to sea surface temperature and export production as derived from sediment trap data. *Marine Micropaleontology*, *55*(1–2), 75–105. https://doi.org/10.1016/j.marmicro.2005.01.002